

Comparative analysis of silver nanoparticles synthesized by Gram-positive and Gram-negative bacteria: assessing their efficacy in dye removal and antimicrobial activity (#89500)

1

First submission

Guidance from your Editor

Please submit by **2 Oct 2023** for the benefit of the authors (and your token reward) .



Structure and Criteria

Please read the 'Structure and Criteria' page for general guidance.



Raw data check

Review the raw data.



Image check

Check that figures and images have not been inappropriately manipulated.

If this article is published your review will be made public. You can choose whether to sign your review. If uploading a PDF please remove any identifiable information (if you want to remain anonymous).

Files

Download and review all files from the [materials page](#).

9 Figure file(s)

5 Table file(s)

1 Raw data file(s)



Structure and Criteria

Structure your review

The review form is divided into 5 sections. Please consider these when composing your review:

1. BASIC REPORTING
2. EXPERIMENTAL DESIGN
3. VALIDITY OF THE FINDINGS
4. General comments
5. Confidential notes to the editor






 You can also annotate this PDF and upload it as part of your review

When ready [submit online](#).





Editorial Criteria

Use these criteria points to structure your review. The full detailed editorial criteria is on your [guidance page](#).

BASIC REPORTING

-  Clear, unambiguous, professional English language used throughout.
-  Intro & background to show context. Literature well referenced & relevant.
-  Structure conforms to [PeerJ standards](#), discipline norm, or improved for clarity.
-  Figures are relevant, high quality, well labelled & described.
-  Raw data supplied (see [PeerJ policy](#)).

EXPERIMENTAL DESIGN

-  Original primary research within [Scope of the journal](#).
-  Research question well defined, relevant & meaningful. It is stated how the research fills an identified knowledge gap.
-  Rigorous investigation performed to a high technical & ethical standard.
-  Methods described with sufficient detail & information to replicate.

VALIDITY OF THE FINDINGS

-  Impact and novelty not assessed. *Meaningful* replication encouraged where rationale & benefit to literature is clearly stated.
-  All underlying data have been provided; they are robust, statistically sound, & controlled.
-  Conclusions are well stated, linked to original research question & limited to supporting results.



The best reviewers use these techniques

Tip

Example

Support criticisms with evidence from the text or from other sources

Smith et al (J of Methodology, 2005, V3, pp 123) have shown that the analysis you use in Lines 241-250 is not the most appropriate for this situation. Please explain why you used this method.

Give specific suggestions on how to improve the manuscript

Your introduction needs more detail. I suggest that you improve the description at lines 57- 86 to provide more justification for your study (specifically, you should expand upon the knowledge gap being filled).

Comment on language and grammar issues

The English language should be improved to ensure that an international audience can clearly understand your text. Some examples where the language could be improved include lines 23, 77, 121, 128 – the current phrasing makes comprehension difficult. I suggest you have a colleague who is proficient in English and familiar with the subject matter review your manuscript, or contact a professional editing service.

Organize by importance of the issues, and number your points

1. Your most important issue
2. The next most important item
3. ...
4. The least important points

Please provide constructive criticism, and avoid personal opinions

I thank you for providing the raw data, however your supplemental files need more descriptive metadata identifiers to be useful to future readers. Although your results are compelling, the data analysis should be improved in the following ways: AA, BB, CC

Comment on strengths (as well as weaknesses) of the manuscript

I commend the authors for their extensive data set, compiled over many years of detailed fieldwork. In addition, the manuscript is clearly written in professional, unambiguous language. If there is a weakness, it is in the statistical analysis (as I have noted above) which should be improved upon before Acceptance.

Comparative analysis of silver nanoparticles synthesized by Gram-positive and Gram-negative bacteria: assessing their efficacy in dye removal and antimicrobial activity

Bhakti Patel ^{Equal first author, 1}, **Virendra Kumar Yadav** ^{Equal first author, 1}, **Reema Desai** ¹, **Shreya Patel** ¹, **Nisha Choudhary** ¹, **Rajat Patel** ¹, **Deepak Balram** ², **Kuang-Yow Lian** ², **Dipak Kumar Sahoo** ^{Corresp., 3}, **Ashish Patel** ^{Corresp. 1}

¹ Department of Life Sciences, Hemchandracharya North Gujarat University, Patan, Gujarat, India

² Department of Electrical Engineering, National Taipei University of Technology, Taipei, Taiwan

³ Department of Veterinary Clinical Sciences, Iowa State University, Ames, Iowa, United States

Corresponding Authors: Dipak Kumar Sahoo, Ashish Patel
Email address: dsahoo@iastate.edu, uni.ashish@gmail.com

In the last decade nanotechnology and nanoparticles have drawn a huge attention of the scientific community in the whole world. The synthesis of nanoparticles by chemical and physical approaches is nonenvironmental friendly and expensive. So, microbial approaches are the most eco-friendly, and biocompatible. In the present research work, investigators have synthesized silver nanoparticles (AgNPs) by using *Klebsiella pneumoniae*, *Micrococcus luteus*, and *Enterobacter aerogenes* and studied their morphological, chemical and elemental properties by using UV-Vis spectroscopy, Fourier transform-infrared spectroscopy (FTIR), X-ray diffraction (XRD), Field emission scanning electron microscope (FESEM) and energy-dispersive spectroscopy (EDX). The UV-Vis spectra show absorbance peaks at 475 nm, 428 nm, and 503 nm for AgNPs synthesized by, *K. pneumoniae*, *M. luteus*, and *E. aerogenes* respectively. The XRD showed the crystalline nature of the synthesized AgNPs, having peaks at 26.2°, 32.1°, and 47.2°, while the FTIR showed bands at 599 cm⁻¹, 963 cm⁻¹, 1693 cm⁻¹, 2299 cm⁻¹, 2891 cm⁻¹, and at 3780 cm⁻¹ for all the types of AgNPs. The FTIR indicated the presence of biomolecules of bacteria with the developed AgNPs. The size of the silver nanoparticles varies from 10 nm to several microns while the shape varies from spherical to porous sheets-like structure. The percentage of Ag varied from 37.8% (wt.%) to 61.6% i.e., highest in AgNPs-K, and lowest in AgNPs-M. Further, all three types of AgNPs were evaluated for the removal of methyl orange dyes from the simulated wastewater where the maximum dye removal percentage was 19.24% at 120 minutes by AgNPs-M. Finally, all three types of AgNPs were assessed for their potential for antibacterial activity against Gram-positive (*Bacillus subtilis*, *Bacillus cereus*, and *Bacillus megaterium*) and Gram-negative bacteria (*Enterococcus fecalis*) out of which the maximum zone of inhibition was 12 mm against *B. megaterium* for the AgNPs-M.

Comparative analysis of silver nanoparticles synthesized by Gram-positive and Gram-negative bacteria: assessing their efficacy in dye removal and antimicrobial activity

Bhakti Patel^{1†}, Virendra Kumar Yadav^{1†}, Reema Desai¹, Shreya Patel¹, Nisha Choudhary¹, Rajat Patel¹, Deepak Balram², Kuang-Yow Lian², Dipak Kumar Sahoo^{3*}, and Ashish Patel^{1*}

¹ Department of Life Sciences, Hemchandracharya North Gujarat University, Patan 384265, Gujarat, India

² Department of Electrical Engineering, National Taipei University of Technology, No. 1, Section 3, Zhongxiao East Road, Taipei 106, Taiwan

³ Department of Veterinary Clinical Sciences, College of Veterinary Medicine, Iowa State University, Ames, Iowa, USA

Correspondence: dsahoo@iastate.edu (D.K.S.); uni.ashish@gmail.com (A.P.)

[†] These authors contributed equally to this work.

Abstract

In the last decade nanotechnology and nanoparticles have drawn a huge attention of the scientific community in the whole world. The synthesis of nanoparticles by chemical and physical approaches is nonenvironmental friendly and expensive. So, microbial approaches are the most eco-friendly, and biocompatible. In the present research work, investigators have synthesized silver nanoparticles (AgNPs) by using *Klebsiella pneumoniae*, *Micrococcus luteus*, and *Enterobacter aerogenes* and studied their morphological, chemical and elemental properties by using UV-Vis spectroscopy, Fourier transform-infrared spectroscopy (FTIR), X-ray diffraction (XRD), Field emission scanning electron microscope (FESEM) and energy-dispersive spectroscopy (EDX). The UV-Vis spectra show absorbance peaks at 475 nm, 428 nm, and 503 nm for AgNPs synthesized by, *K. pneumoniae*, *M. luteus*, and *E. aerogenes* respectively. The XRD showed the crystalline nature of the synthesized AgNPs, having peaks at 26.2°, 32.1°, and 47.2°, while the FTIR showed bands at 599 cm⁻¹, 963 cm⁻¹, 1693 cm⁻¹, 2299 cm⁻¹, 2891 cm⁻¹, and at 3780 cm⁻¹ for all the types of AgNPs. The FTIR indicated the presence of biomolecules of bacteria with the developed AgNPs. The size of the silver nanoparticles varies from 10 nm to several microns while the shape varies from spherical to porous sheets-like structure. the percentage of Ag varied from 37.8% (wt.%) to 61.6% i.e., highest in AgNPs-K, and lowest in AgNPs-M. Further, all three types of AgNPs were evaluated for the removal of methyl orange dyes from the simulated wastewater where the maximum dye removal percentage was 19.24% at 120 minutes by AgNPs-M. Finally, all three types of AgNPs were assessed for their potential for antibacterial activity against Gram-positive (*Bacillus subtilis*, *Bacillus cereus*, and *Bacillus megaterium*) and Gram-negative bacteria (*Enterococcus faecalis*) out of which the maximum zone of inhibition was 12 mm against *B. megaterium* for the AgNPs-M.

KEYWORDS silver nanoparticle, methyl orange, bioremediation, antimicrobial, zone of inhibition

1. Introduction

The rapid industrialization in India as well as in the whole world has increased the use of different synthetic dyes. Some of the dyes may cause harm to aquatic life and cause diseases in living organisms (Patel et al., 2022). Dyes are mainly used in textile industries for coloring fabric, so textile industrial wastewater contains a huge concentration of dyes in it (Al-Tohamy et al., 2022). The prolonged and continuous contamination of textiles and other dyes in the water bodies may lead to water pollution. It also gives rise to many diseases in humans due to its carcinogenic properties. Dyes present in textile effluent can be removed by using various chemical approaches. The chemical approaches include precipitation, coagulation (Yadav et al., 2022b), flocculation, membrane filtration (nanofiltration, ultrafiltration) (Chahar et al., 2023), reverse osmosis, adsorption, etc. (Robati et al., 2016). The biological approach involves the utilization of microbes for dye remediation, either in the natural sites or in the bioreactor (Das and Mishra, 2017). The biological also involves biosorbents for the remediation of dyes from the wastewater (Modi et al., 2023). Such processes are economical if the biosorbents are developed from agricultural waste etc. All of these processes have certain advantages and disadvantages but adsorption is a very simple, effective, and economical approach. The adsorbent in the adsorption process could be easily surface functionalized by various chemical compounds for the targeted removal of pollutants (Harja et al., 2022). The various adsorbents which are commonly used are alumina, silica (Imoisili et al., 2022; Yadav et al., 2022a, 2023b), zeolites (Murukutti and Jena, 2022), coal fly ash, magnetite, maghemite, zinc oxide (Soltani et al., 2023), and titania (Dash et al., 2018; Yang et al., 2022). When these adsorbents are used in their nanoform they become highly effective due to their high

surface area to volume ratio (SVR), and high surface energies (Yadav et al., 2022c, 2023a; Amari et al., 2023). Both nanoparticle nanotechnology has played an important role in the last decade in the remediation of textile dyes from contaminated water efficiently. To date, both metal and metal oxide NPs have been used for dye removal from wastewater. Out of these one such particle is silver NPs (AgNPs)(Nisha et al., 2017) which is used by several investigators for the dye removal from wastewater. Nanoparticles are materials whose sizes fall in the range of 1 to 100 nm. Due to its high surface area, it has gained huge popularity in the field of adsorption-based remediation of water pollutants. Moreover, NPs have high adsorption capacity due to this property dye easily gets adsorbed on the surface of nanoparticles. Nanoparticles of silver can be used for dye removal (Dalvand et al., 2020; Degefa et al., 2021; Tarekegn et al., 2021).

Currently, silver NPs are synthesized by chemical, physical, and biological approaches (Bouafia et al., 2021), out of which biological and specifically, microbial synthesis of AgNPs is of high significance due to the presence of various functional on the surface of AgNPs (Naganthran et al., 2022). Among all the microorganisms, bacterial synthesis is preferred due to their easy handling, and short time duration for their growth in comparison to algae and fungi (Choudhary et al., 2023). Bacteria are capable of synthesizing AgNPs by means of various microbial proteins and enzymes which act as reducing agents, capping, and stabilizing agents. Vimalanathan and their team synthesized AgNPs by using wet biomass of the *Micrococcus luteus* (Vimalanathan et al., 2013).

To date several investigators have used bacteria for the synthesis of AgNPs for instance, Esmail and their team reported the synthesis of less than 25 nm AgNPs, by using the supernatant of the bacteria *Bacillus* ROM6. This particular bacterium was isolated from the Zarshouran gold mine, in South Korea. Further, the synthesized AgNPs were used as an antimicrobial agent against *S. aureus*, *E. coli*, *P. aeruginosa*, and *Acinetobacter baumannii* (Esmail et al., 2022).



Saeed and their team synthesized 5-10 nm, spherical-shaped AgNPs by using secondary metabolites of *E. coli*, *Exiguobacterium aurantiacum*, and *Brevundimonas diminuta* with NCBI accession number MF754138, MF754139, and MF754140 respectively. Further, the investigator observed the antimicrobial activity of the synthesized AgNPs against methicillin-resistant *Staphylococcus aureus* (MRSA) and several other multiple drug resistance (MDR) bacteria where the zone of inhibition was varying from 10 mm to 28 mm. Further, the investigators used AgNPs against plant pathogens (Saeed et al., 2020). A team led by Cekuolyte synthesized morphologically different types of AgNPs by using different strains of *Geobacillus* bacteria, namely, 18, 25, 95, and 612 (Cekuolyte et al., 2023).



From the very beginning of civilization, the antimicrobial effect of silver is known due to which it was used for various applications (Kyung et al., 2008). Being a heavy metal, it coagulates the enzymes and proteins of the microorganism, thus inhibiting them and ultimately killing them (Betts et al., 2021). So, the nanosized silver can increase the efficiency of antimicrobial activity due to its small size, and high surface area as being smaller in size it may enter the microorganism through the cell wall leading to the inhibition and killing of the microorganism (Karunakaran et al., 2017). From the various pieces of literature, it has been found that AgNPs have a broad spectrum of antimicrobial activity (Singh and Mijakovic, 2022) which continuously releases silver ions, thus acting as an antimicrobial agent. The antimicrobial activity of the nanoparticles or AgNPs depends on their size and surface area of AgNPs (Kalwar and Shan, 2018). The smaller size of AgNPs may facilitate their entry inside the microbes and exhibit their antimicrobial effect. There are several examples where AgNPs have been used as an antimicrobial agent.



A team led by Raza observed the antimicrobial activity of AgNPs on the *Enterococcus faecalis* ATCC 29212. The AgNPs here were synthesized by using *Aspergillus fumigatus* KIBGE-

IB33. Further investigators developed a nanocomposite by using the AgNPs with chitosan and observed that the lowest minimum inhibitory concentration of the nanocomposite system was 1.56 $\mu\text{g mL}^{-1}$ against *Enterococcus faecalis* ATCC 29212 (Raza et al., 2021). Srinivasan and their team, synthesized AgNPs by using a bioluminescent bacterium (*Vibrio campbellii*). Further, the investigators assessed the antibacterial and antioxidant activity of the synthesized AgNPs. The antibacterial activity was tested against a number of Gram-negative pathogenic bacteria like *Aeromonas hydrophila* MTCC 1739, *K. pneumoniae* MTCC4030, *Klebsiella oxytoca* MTCC 3030, and *Pseudomonas aeruginosa* MTCC 1934. The AgNPs exhibited antioxidant activity by strong scavenging actions on 2,2-diphenyl-1-picrylhydrazyl (DPPH) (61.88%) and hydrogen peroxide (53.48%) free radicals (Srinivasan et al., 2022).

In the present research work, investigators have isolated three different bacterial strains from the soil samples. Further, the bacterial strains were used for the synthesis of silver nanoparticles under normal laboratory conditions. The synthesized silver nanoparticles were characterized by Fourier transform infrared spectroscopy, UV-Vis spectroscopy, X-ray diffraction pattern, Field emission scanning electron microscopy, and Energy dispersive X-ray spectroscopy for the confirmation of formation of silver NPs and purity. One of the objectives was to observe the morphological diversity in the synthesized AgNPs by the bacteria. One more objective was to assess the potential of AgNPs as an adsorbent for the remediation of methyl orange dye from the simulated wastewater. One final objective was to evaluate the potential of the synthesized AgNPs as an antibacterial agent against gram-positive (*B. subtilis*, *B. cereus*, and *B. megaterium*) and gram-negative bacteria (*Enterococcus faecalis*).

2. Materials and methods

2.1. Materials

Silver nitrate (SRL, Gujarat, India), nutrient agar media (Himedia, Mumbai, India), nutrient broth (Himedia, Gujarat, India), antibiotic assay media (Himedia, Mumbai, India), Ethanol (Shenzhen, China), Whatman filter paper no 42. (Axiva, Mumbai, India), Methyl orange (Loba, Chemie, Gujarat, India). All the chemicals were of analytical grade except silver nitrate and Methyl orange dye (LR grade), double distilled water (ddw).

2.2. Methods

2.2.1. Isolation and screening of bacteria from the Soil

The soil was collected from the various parts of the Industrial sites and coastal areas of Gujarat, India, in sterilized autoclavable bags. Further, it was stored in the refrigerator in the laboratory. About 1 gram of soil sample was taken in a sterile test tube having 10 mL of ddw. Further serial dilution was performed to obtain the pure and isolated colonies. Further, the isolated colonies were screened for the synthesis of AgNPs.

2.2.2. Preparation of 20 Mm aqueous solution of silver nitrate solution

A 20 mM aqueous solution of silver nitrate solution was prepared by adding it into a 500 mL ddw in an amber bottle. The silver nitrate solution was kept for the future.

2.2.3. Synthesis of silver nanoparticles from bacteria

The isolated bacterial colonies were grown on nutrient agar plates. Further, for the mass production of bacteria, a loopful culture was inoculated into the nutrient broth in an Erlenmeyer flask. All three flasks containing nutrient broth were incubated in an incubator shaker at 37 °C for 24 hours at 120 rpm. Further, after 24 hours, the bacterial colonies were taken out and centrifuged at 5000 rpm for 10 minutes. The bacterial supernatant was retained while the bacterial pellet was discarded.

Further, about 100 mL of all three bacterial supernatants were taken separately in three amber bottles, and to each bottle, about 100 mL of silver nitrate solution was added. After that, all three flasks including the control which has ddw instead of bacterial supernatant were kept under dark conditions for 2-3 days, and color change was continuously monitored. Initially, the color of the silver nitrate aqueous solution was pale while, after the addition of bacterial supernatant, the color tuned to milky white in appearance. Finally, after 2-3 days, the color of the three bottles changed from milky white to reddish brown in color indicating the formation of AgNPs. The mixture from each bottle was transferred to the centrifugation tubes separately and centrifuged at 5000 rpm for 10 minutes. The supernatant was discarded while the solid particle was retained. Further, the pellet was washed 2-3 times with distilled water and once with ethanol. All three types of silver NPs were then transferred into different Petri plates and kept for drying in an oven at 50-60 °C till complete dryness. **Figure 1** is showing the schematic steps involved in the formation of AgNPs from the bacterial supernatant.

FIGURE 1 Schematic diagram for the synthesis of AgNPs using bacterial supernatant.

2.2.4. Preparation of aqueous solution methyl orange dye

A 50-ppm aqueous solution of methyl orange (MO) dye was prepared by adding 50 mg of MO dye powder granules into the 1000 mL double distilled water. The aqueous solution was kept on a magnetic stirrer along with vigorous stirring (250 rpm) for the complete dissolution of the dye granules. Further, the aqueous solution was filtered through a Whatman filter paper no. 42 in order to remove the impurities. Finally, the dye sample was stored in a reagent bottle for future use.

2.2.5. Batch study of adsorption of methyl orange dye

About 100 mL of an aqueous solution of MO dye was taken from the stock solution into three different glass beakers of appropriate volume. All these three glass beakers were placed on a magnetic stirrer to which 1 mg AgNPs of each type was added to different glass beakers. The interaction between the AgNPs and MO dye was carried out by agitation at 400 rpm for all three flasks. Further, an aliquot (2-3 mL) was collected from all three glass beakers at 0 minutes, 30 mins, 60 mins, 90 mins, and 120 mins. All the collected samples were then analyzed by the UV-Vis spectrophotometer for the concentration of dye samples. The UV-Vis absorbance maxima of MO dye are 520 ± 15 nm. Further, the percentage removal of MO dye was calculated by using the following formula as provided by Yadav et al.; -

$$\% \text{ Dye removal} = \frac{C_o - C_t}{C_o} \times 100 \quad (1)$$

Where, C_o = initial dye concentration,

C_t = dye concentration at a specific time

2.2.6. Antimicrobial activity of silver nanoparticles

The antimicrobial activity of the synthesized AgNPs was carried out by the disk diffusion method (Yassin et al., 2022). Firstly, antibiotic assay media was prepared and poured on the Petri plates. Once the media was solidified, in the Petri plates, the tested bacterial organism was swabbed on the Petri plates. After a while, disks of a specific size (8 mm diameter) were cut and dipped into different concentrations of AgNPs in ddw in a reagent vial, prepared by different bacterial strains. Further, all the reagent vials were kept for sonication, for 15-20 minutes in an ultrasonicator (Lequitron). After, sonication the disks were taken out with the help of forceps and transferred into the lid of the Petri plates and kept in a hot air oven at 40-50 °C for drying. Finally, the antibiotic

assay plates were swabbed with the different bacterial colonies with the help of a sterile cotton swab. Once the bacterial colonies were dry well was punched onto the surface of the plates with the help of a sterile cork borer. Further, about 10 μ L AgNPs suspension in ddw was poured into the wells of Petri plates with the help of a micropipette. Finally, the Petri plates were placed in a hot air oven/ incubator at 37 °C for 24 hours. After 24 hours antibiotic assay plates were observed for the evaluation of antimicrobial activity of the synthesized AgNPs. The zone of inhibition (ZOI) was measured by using a measurement scale against the light and recorded in mm (Ballén et al., 2021).

3. Characterization of silver nanoparticles

3.1. UV-Visible spectroscopy

The UV-Vis measurement of AgNPs was done by dispersing about 1 mg of all three types of AgNPs in 5 mL ddw in three different test tubes. All these three tubes having AgNPs were sonicated in an ultrasonicator (Lequitron) for 10 minutes to disperse the particles. The well-dispersed samples were then taken in a quartz cuvette and the UV-Vis measurement was done in the range of 200-800 nm at a resolution of 1 nm, by using a UV-Vis spectrophotometer (UV 1800, Shimadzu spectrophotometer, Japan).

3.2. FTIR

The FTIR measurement was done to identify the various functional groups present in the bacterially synthesized AgNPs. The FTIR measurement was done by using a solid KBr pellet technique where the pellets were prepared by mixing 2 mg AgNPs and 198 mg KBr for each sample. The FTIR measurement was made in the mid-IR region 599-4000 cm^{-1} at a resolution of 2 cm^{-1} by using a spectrum S6500 instrument (Perkin-Elmer, USA).

3.3. XRD

The XRD patterns for all three types of AgNPs samples were recorded by using Miniflex 800 (Rigaku, Netherlands) instrument equipped X'celerator in order to reveal the crystallinity. XRD patterns were recorded in the 2-theta range of 20-70 by using a filter K-beta (x1) with a step size of 0.02 and a time of 5 seconds per step, scan speed/duration time: 10.0 deg/min., step width: 0.0200 deg. at 30 kV voltage and a current of 2 mA.

3.4. FESEM-EDS

The morphological analysis of all three types of AgNPs was carried out by using a Novo Nanosem, Fei 450, (USA). The dry AgNPs were loaded on the carbon tape with the help of a fine brush which in turn was placed on the aluminum stub holder. All the samples were exposed for gold sputtering. The elemental analysis of AgNPs was analyzed by using an Oxford-made energy-dispersive X-ray spectroscopy (EDS) analyzer attached to the FESEM at variable magnifications and at 20 kV.

4. Results and discussion

4.1. Mechanism of formation of AgNPs by bacteria

The bacterial strains i.e., *K. pneumoniae*, *M. luteus*, and *E. aerogenes* have numerous microbial proteins and enzymes which help in the bioreduction of Ag^{2+} ions into Ag^0 (Ballén et al., 2021). The actual mechanism of biosynthesis of AgNPs by bacteria is well described in the literature. It is a very simple and easy mechanism where the oxidized silver ions get two electrons from any of the microbial proteins and enzymes and gets reduced to the stabilized Ag^0 . When the AgNO_3 aqueous solutions are mixed with the bacterial culture or with their supernatant the enzymes and proteins present in the supernatant reduce the Ag^{2+} ions into Ag^0 . So, during this step, the previously milky color of the aqueous silver solutions gets converted to red color, which indicates

the formation of silver NPs in the medium. Moreover, these biomolecules may also act as stabilizing and capping agents for the synthesized AgNPs (Giri et al., 2022; Terzioğlu et al., 2022). **Figure 2** is showing the mechanism involved in the synthesis of AgNPs from the bacteria. Here the color of the medium changed from milky white to dark brown within 2-3 days. A similar color change (from yellow to brown) was also previously reported by Sayyid and Zghair (2021) during the synthesis of AgNPs by *K. pneumoniae* isolated from humans and sheep (Sayyid and Zghair, 2021). Saleh and Alwan used *K. pneumoniae* culture supernatant for the biosynthesis of AgNPs (Saleh and Khoman Alwan, 2020). Previously Javaid and their team also suggested a similar pathway for the formation of AgNPs from the bacteria via aa via NADH-dependent nitrate reductase enzyme (Javaid et al., 2018). **Table 1** is showing the major microbial proteins and enzymes present in *K. pneumoniae*, *M. luteus*, and *E. aerogenes*.

TABLE 1 The major microbial proteins and enzymes present in *K. pneumoniae*, *M. luteus*, and *E. aerogenes*.

FIGURE 2 Schematic diagram for the formation of AgNPs from silver ions by bacteria via NADH-dependent nitrate reductase enzyme.

4.2. UV-Vis analysis for preliminary confirmation of the formation of AgNPs

The UV-Vis measurement was done for the preliminary confirmation of the formation of AgNPs from the bacterial strains. **Figure 3** is showing a typical UV-Vis spectra of AgNPs synthesized by bacteria. All of them exhibit a peak in the range of 350-450 nm, which indicates the formation of AgNPs. Earlier, Saleh and Alwan obtained a peak at 432 nm for the *K. pneumoniae* supernatant-mediated synthesized AgNPs. Previously a team led by Vimalanathan obtained an absorbance peak at 420 and 440 nm for the AgNPs synthesized by *M. luteus* (Vimalanathan et al., 2013). Hamaouda

and their team synthesized AgNPs by using cyanobacterium *Oscillatoria limnetica* and obtained a UV-Vis absorbance peak at 450 nm (Hamouda et al., 2019). Kumar and Dubey synthesized AgNPs by using an endophyte *Enterobacter roggenkampii* BLS02 from *Barleria lupulina* also obtained a UV-absorbance peak in the same region (Kumar and Dubey, 2022). Kalpana and their team obtained UV-Vis absorbance at 405–407 nm for the AgNPs synthesized with variable ratio of bacterial supernatant (*Klebsiella pneumoniae*) and AgNO₃ solution. The investigators concluded that when the ratio of AgNO₃: bacterial supernatant was about 4:6, then the absorption intensity was higher so they formed AgNPs. Further concluded that the UV–Vis absorption is directly proportional to the amount of substance at their maximum absorption spectra i.e., higher yield of AgNPs and efficient production of AgNPs even at lower concentrations of silver nitrate can be obtained when more amount of cultural filtrate is used. The investigator further also showed that the amount of reducing agents plays an important role in the formation of AgNPs (Kalpana and Lee, 2013).

FIGURE 3 UV-Vis measurement of AgNPs synthesized by bacteria.

4.3. Identification of functional groups of silver NPs by FTIR

The **Figure 4** is showing the FTIR spectra of all the AgNPs (AgNPs-K, AgNPs-M, and AgNPs-E) synthesized by bacteria, which was done to identify the various functional groups present AgNPs. All the samples have a common band at 599 and 963, 1299, 1349, 1693, 2299, 2891, and 3780 cm⁻¹. The band at 599 cm⁻¹ is attributed to the metallic Ag. The band at 963 cm⁻¹ is attributed to the amide V band arising due to out-of-plane NH bending of peptide linkages (Kalpana and Lee, 2013). A small intensity band at 1051 cm⁻¹ is attributed to the primary amine C–N stretch. Another small intensity band at 1349 cm⁻¹ in all the samples is attributed to the C–C bond. A small intensity band in all the samples at 1699 cm⁻¹ is attributed to the OH group in the samples. Moreover, this band is also attributed to the C=O stretching of amide I bands of peptide linkage. The band at 1229

cm⁻¹ is attributed to the CN stretching of peptide linkage. The band at 1349 cm⁻¹ is attributed to the (C–C) stretching vibration of aliphatic amines., which was earlier also reported by Ibrahim and their team at 1359 cm⁻¹ from the AgNPs synthesized by endophytic bacteria (Ibrahim et al., 2019). All the samples exhibit an atmospheric carbon band at 2891 cm⁻¹ is attributed to the methylene C–H asymmetric or symmetric stretch. All the samples showing a small band from 3400 cm⁻¹ to 3800 cm⁻¹ centered at 3780 cm⁻¹ are attributed to the -OH molecule.

Earlier, Saleh and Alwan obtained four distinct peaks for the AgNPs synthesized by *K. pneumoniae* at 3332.78, 2115.35, 1635.60, and 1096.92 cm⁻¹. The investigators concluded that the band obtained at 3332.78 cm⁻¹ is due to the stretching vibration of the OH bond of alcohol and phenols. The band at 2115.35 cm⁻¹ was found due to the C-H stretching of the methylene groups of protein and to the N-H stretching of amine salt. The band at 1635.60 cm⁻¹ was attributed to carbonyl groups (C=O) of the amino acid residues while the band at 1096.92 cm⁻¹ was attributed to the (C-O) stretching of alcohols and esters, carboxylic acids, and C–N stretching of aliphatic amines (Saleh and Khoman Alwan, 2020). Based on the above information it was further concluded that the presence of protein in the supernatant acts as a stabilizing and capping agent for stabilization which bind to the synthesized AgNPs through free cysteine or amine groups in proteins (Saleh and Khoman Alwan, 2020). Previously, Kalpana and Lee (2013) also obtained bands for the AgNPs synthesized by using a culture of simulated microgravity-grown *K. pneumoniae*. The investigators obtained major intensity band at 2964.55 cm⁻¹, 1262.22 cm⁻¹, 1095.89 cm⁻¹, 1021.96 cm⁻¹, 800.73 cm⁻¹, and small intensity bands at 2960.64 cm⁻¹, 1650.01 cm⁻¹, 865.33 cm⁻¹, 701 cm⁻¹ and 477.07 cm⁻¹.

FIGURE 4 FTIR spectra of AgNPs synthesized by bacteria.

In the current investigation also, authors have obtained bands for the *K. pneumoniae* synthesized AgNPs at 599, 963, 1229, 1693, 2891, and 3780 cm^{-1} which were corresponding to the bands obtained by Kalpana and Lee 2013 (Kalpana and Lee, 2013). Peris and their team also obtained four prominent FTIR bands at 1643, 1586, 1397, and 1042 cm^{-1} and concluded that the AgNPs synthesized by bacteria have enhanced stability because of the coating of AgNPs by bacterial and media components (Peiris et al., 2018). AgNPs-M. and AgNPs-E have almost similar bands to that of AgNPs-K which could vary only in their intensity which could be weak or strong.

4.4. Phase identification of silver nanoparticles by XRD

The XRD investigation was carried out to identify the crystalline phase of the AgNPs. A typical XRD pattern of all the bacterially synthesized AgNPs is shown in **Figure 5**. All the AgNPs exhibit three characteristic peaks of silver NPs at 27.6°, 32.1°, and 46.2°, and three small intensity peaks at 54.7°, and 57.4° and 76.7°. The major intensity peaks in all three types of bacterially synthesized AgNPs are at 32.1° followed by 46.2° and 27.6°. The XRD planes in all three types of AgNPs were 101, 111, 200, 220, and 311 as matched with the Joint Committee on Powder Diffraction Standards (JCPDS) 03-0921. In the current investigations, the authors obtained diffraction peaks at 27.6°, 32.1°, and 46.2°, and small diffraction peaks at 54.7°, 57.4° and 76.7 for the AgNPs-K. AgNPs-M has also the same peaks as that of AgNPs-K, i.e., at 27.6, 32.1, 46.2 and 54.7, and 57.4°. All the XRD peaks for AgNPs-M were of almost the same intensity except for 27.6° which was comparatively stronger than the AgNPs-K. The XRD peaks for AgNPs-E were also at the same places as that of AgNPs-M and AgNPs-K, but the peak at 27.6 was of strong intensity than the AgNPs-K and weaker than the AgNPs-M. Moreover, the peak at 46.2 in both AgNPs-M and AgNPs-E was stronger than the AgNPs-K. Further, the peaks at 54.7 (311) and 57.4 (222) were

like a small broad hump in both AgNPs-K and AgNPs-M but these two peaks were sharper in the AgNPs-E.

The results were in close agreement with the previous results obtained by Kalpana and Lee and Ibrahim et al., 2019. Kalpana and Lee obtained diffraction peaks at 37.76°, 45.87, 64.08°, and 77.11° which was indicated by the (111), (200), (220), and (311) reflection of metallic Ag. The data obtained here was matched with the database of the JCPDS file no 03-0921 (Kalpana and Lee, 2013). Ibrahim and their team obtained diffraction peaks for the AgNPs synthesized by an endophytic bacteria *Bacillus siamensis* strain C1 at 27.81, 32.34, 46.29, 57.47, and 77.69°, corresponding to (101), (111), (200), (220), and (311) crystal planes, respectively, for the AgNPs (Ibrahim et al., 2019). Previously Vimalanathan and their team also obtained similar results where the major peaks were at 28, 32, and 47°, and two small intensity peaks at 55° and 57°. The investigators also obtained a small diffraction peak at 76°.

FIGURE 5 XRD pattern of silver nanoparticles synthesized by bacteria.

The crystalline size of the synthesized silver nanoparticle is determined using the Scherrer formula as given in equation (2),

$$D = \frac{k\lambda}{\beta \cos \theta} \quad (2)$$

Where D is crystalline size, k is constant (0.9), and β indicates the FWHM values of the diffracted peaks.

The highest intensity peak was used to find all the parameters in the Scherrer equation. The Gaussian peak fits were used to find the FWHM values and exact theta values. The calculated crystalline size was found around 16.88 nm, 18.00 nm, and 16.44 nm for AgNPs-K, AgNPs-M,

and AgNPs-E. Therefore, it is well examined that the synthesized AgNPs showed a crystalline nature and 16.88 nm, 18.00 nm, and 16.44 nm crystalline size.

4.5. Morphological analysis of silver nanoparticles by FESEM and elemental analysis by EDS

Figure 6a-6f shows FESEM micrographs of AgNPs synthesized by *K. pneumoniae* (AgNPs-K).

Figure 6a&b show a porous flakes-like structure that is embedded with bright color AgNPs.

Figure 6c&d clearly show rhombohedral-shaped AgNPs, whose size is varying from 22-66 nm.

These two images clearly show that the AgNPs are embedded in porous sheet-like structures.

Figure 6e&f show aggregated spherical-shaped structures. Previously several investigators have

shown similar morphology for the bacterially synthesized AgNPs. **Figure 6g** shows the EDS spot

of the AgNPs-K while **Figure 6h** exhibits EDS spectra and elemental table of the AgNPs-K.

Figure 6h shows spectra of Ag, Cl, Na, P, S, C, O, and N. Out of all these the major elements were

mainly Ag (37.8% At wt.), Cl (29.8%), Na (21.8) C (7 %) and O (2.8%). In addition to this rest of

the elements were present in trace amounts i.e., P, S. N was not detected in the AgNPs-K. The

major impurities in the synthesized AgNPs-K are NaCl which alone comprises 50% this indicates

the improper washing of the samples. Moreover, these two may also come from the nutrient broth

used for growing the bacteria. While the presence of C, S, and P indicates the presence of

biomolecules with the synthesized AgNPs-K. Earlier Sayyid and Zghair (2021) reported cube-

shaped to irregular heterogeneous forms of AgNPs synthesized by *K. pneumoniae* whose average

size was 40.47 nm (Sayyid and Zghair, 2021). Moreover, investigators further observed that the


morphology by TEM was a pseudo-spherical shape of size 40-80 nm.

FIGURE 6 FESEM images (a-f), EDS spot (g), and EDS spectra and elemental table (h) for

AgNPs-K. FESEM images (i-l), EDS spot (m) and EDS spectra, and elemental table (n) for

375 AgNPs-M. FESEM images (o-r), EDS spot (s) and EDS spectra, and elemental table (t) for AgNPs-
376 E.

377 Saleh and Alwan (2020) obtained spherical-shaped particles of size m 26.84 to 44.42 nm which
378 were highly aggregated. Further, the investigators concluded the conglomeration of the AgNPs is
379 during the drying process (Saleh and Khoman Alwan, 2020).

380 **Figure 6i-l** shows FESEM micrographs of AgNPs synthesized by the *M. luteus* (AgNPs-M).
381 **Figure 6i&j** shows a high aggregation of the synthesized AgNPs-M. **Figure 6k** and **Figure 6l**
382 show spherical-shaped AgNPs-M whose size is varying from 21-45 nm. **Figure 6m** shows the
383 EDS spot of the AgNPs-M while **Figure 6n** exhibits EDS spectra and elemental table of the
384 AgNPs-M. The EDS spectra of AgNPs-M in **Figure 6n** show peaks for Ag, Cl, Na, P, S, C, O, and
385 N. Out of all these the major elements were mainly Ag (61% At wt.), Cl (21%), C (8.4%), N (3.7%)
386 and O (2.6%). In addition to this  elements were present in the trace amounts. Cl is the major
387 impurity due to improper washing of the final sample. Moreover, it also came from the bacterial
388 media i.e., nutrient broth. While the presence of C, N, S, and P indicates the presence of
389 biomolecules with the AgNPs-M.

390 **Figure 6o-r** shows FESEM micrographs of AgNPs synthesized by *E. aerogenes* (AgNPs-E).
391 **Figure 6o&p** shows a porous flakes-like structure that is embedded with the bright color of
392 AgNPs. **Figure 6q&r** clearly show rhombohedral-shaped AgNPs-E, whose size is varying from
393 24-60. The images clearly show that the AgNPs-E are embedded in the porous flakes-like. The
394 particles are showing high aggregation as evident from the images. **Figure 6s** shows the EDS spot
395 of the AgNPs-E while **Figure 6t** exhibits EDS spectra and elemental table of the AgNPs-E. **Figure**
396 **6t** shows spectra of Ag, Cl, Na, P, S, C, O, and N. Out of all these the major elements were mainly
397 Ag (52.1% At wt.), Cl (21.7%), C (9.8 %) and O (8.2%), Na (4.0%) and N (3.1%). In addition to

this P and S were present in trace amounts whose total composition was near 1.1%. The major impurities in the synthesized AgNPs-E are NaCl which alone comprises 25.7% which indicates the improper washing of the sample. Moreover, these two may also come from the nutrient broth used for growing the bacteria. While the presence of C, S, N, and P indicates the presence of biomolecules with the synthesized AgNPs-E. **Table 2** is showing the major elements present with all three types of AgNPs synthesized by bacteria.

TABLE 2 Comparison between all the elements present in all three types of AgNPs.

From the EDS data of all three types of AgNPs, it was found that Ag was present in the highest percentage in AgNPs-M while at least 37.8% in AgNPs-K. Among all the three types of AgNPs, Cl was present maximum in AgNPs-K while least in AgNPs-M (21.0%). The O was present in the highest amount in AgNPs-E and the least in AgNPs-K i.e., 8.2% and 2.8% respectively. The carbon was highest in AgNPs-E (9.8%) and least 7.0% in AgNPs-K. Out of all the three types of AgNPs, Na was highest in AgNPs-K (21.8%) and least in AgNPs-M (0.4%). Among all the three samples of AgNPs, N was present highest in AgNPs-M (3.7%) and 3.1% in AgNPs-E and it was not detected in AgNPs-K. While P and S were present almost similar in all the samples but least in AgNPs-K i.e., 0.4%.

In the current investigation, the authors have got a broad peak of silver ions at 3 keV in all three types of AgNPs, which confirmed the reduction of Ag^+ to Ag^0 . Moreover, here the authors have mainly got peaks in EDS for Ag, Cl, and C. The peaks for Ag, Cl, and S were consistent with the results obtained for the AgNPs synthesized by endophytic bacteria by Ibrahim and their team. Ibrahim and their team also concluded that the broad peak of silver ions was formed at 3 keV, which indicated the reduction of Ag^+ to Ag^0 (Ibrahim et al., 2019). **Table 3** shows the comparative analysis of the bacterially synthesized AgNPs

TABLE 3 The comparative analysis of the bacterially synthesized AgNPs.

4.6. Remediation of dye by batch adsorption study



Methyl orange dye shows the highest absorbance at a particular wavelength (464 nm) when examined using a UV-Vis spectrophotometer. The dye removal using AgNPs-M shows the highest absorbance of MO dye at 0 min due maximum concentration of dye in a sample. As time increases the concentration of dye in a sample decrease so it shows a gradual decrease in absorbance. So, the lowest concentration of MO was found at 120 min which means that the highest removal of MO dye using AgNPs-M was at 120 min. The highest concentration and absorbance of MO dye at 0 min at a wavelength of 464 nm. The readings at an interval of every 30 min show a slow decrease in the concentration and absorbance of the dye, hence the decrease in the graph can be observed easily as move from 0 min to 120 min. It simply states that by using AgNPs-K this dye can be removed efficiently. The AgNPs-E used for MO dye removal is showing the highest absorbance value at 0 min at 464 nm wavelength and are comparatively decreased after the interval of 30 min. At 60 min the absorbance is decreased when compared to 0 min. After 60 min there was less decrease in absorbance up to 120 min. **Figure 7** shows the MO dye absorbance by UV-Vis spectroscopy at different time intervals.

FIGURE 7 MO dye removal by different types of AgNPs with respect to contact time as measured by UV-Vis spectrophotometer.

4.7. Percentage removal of MR dye by all the AgNPs

AgNPs-M removed MO dye 2.34% at 30 min, 4.37% at 60 min, 14.83% at 90 min, and 19.24% at 120 min. AgNPs-K removes MO dye 1.50% at 30 min, 4.06% at 60 min, 9.56% at 90 min, and 15.03% at 120 min. AgNPs-E removes MO dye 1.52% at 30 min, 2.36% at 60 min, 3.86% at 90

min, and 4.15% at 120 min. By comparing all the AgNPs mention above we can observe that AgNP-M has more efficiency of dye removal and AgNP-E have the least efficiency of dye removal. **Figure 8** shows the percentage removal of MO dye by all three types of AgNPs.

FIGURE 8 Percentage removal of MO dye by all three types of AgNPs.

4.8. Antimicrobial activity of the synthesized AgNPs

AgNPs-K shows a zone of inhibition (ZOI) of 11 mm against *B. megaterium* and *E. fecalis*. *B. subtilis* shows a moderate ZOI of 10 mm when compared with other zones, and *B. cereus* shows a 9 mm ZOI due to the effect of AgNP. Earlier Syaid and Zghair also used the *K. pneumoniae* synthesized AgNPs for the antimicrobial activity against *Staph. aureus* and *Escherichia coli*. The investigators used about 40-50 µg/mL of AgNPs and found that *E. coli* was more susceptible to AgNPs compared to Gram-positive bacteria such as *Staph. aureus*. Further, the investigators suggested that this could be due to variations in the thickness and composition of their cell walls, like peptidoglycan (Sayyid and Zghair, 2021). Saleh and Alwanz (2020) assessed the three concentrations of AgNPs (50, 10, and 150 µg/mL) synthesized from *K. pneumoniae* and evaluated them against *E. coli*, *Ps. aeruginosa*, *Staph. aureus*, and *B. cereus*. Investigators reported that the highest concentration i.e., 150 µg/mL was found most effective against these pathogens in comparison to the 50 and 100 µg/mL. This suggests that the increase in the concentration of AgNPs increases the antibacterial activity (Saleh and Khoman Alwan, 2020).

The use of AgNPs-M for antibacterial activity using different bacteria like *B. subtilis*, *B. cereus*, *B. megaterium*, *E. fecalis* shows different ZOI. AgNPs-M shows a maximum ZOI of 12 mm against *B. megaterium* and a minimum ZOI against *B. cereus* of 8 mm. It shows a moderate ZOI of 9 mm against *E. fecalis* and 11 mm against *B. subtilis*. The *B. megaterium* was more susceptible

than *E. fecalis* and *B. subtilis* moderately susceptible, and *B. cereus* was less susceptible to the AgNPs-M.

B. cereus gives a greater ZOI of 11 mm due to the effect of AgNPs-E the lowest ZOI is observed against *B. megaterium* which is 8 mm and also shows a 10 mm ZOI by *B. subtilis* and *E. fecalis*.

Fig 9 is showing the antibacterial activity of Petri plates of the AgNPs against tested bacterial species. **Table 4** is showing the ZOI, tested bacterial species, and AgNPs, while, **Table 5** is showing comparison of antibacterial activity of current investigation with previously reported studies.

FIGURE 9 Antibacterial activity, zone of inhibition of AgNPs synthesized against the tested bacterial species.

TABLE 4 The ZOI, tested bacterial species, against different bacterially synthesized AgNPs.

TABLE 5 Summarized form of comparison of antibacterial activity of AgNPs of earlier reported work and current investigation.

The difference between the antibacterial effect against Gram-positive and Gram-negative bacteria over here might be due to the morphological differences in both types of bacteria (Jubeh et al., 2020). Gram-positive bacteria have a thick peptidoglycan layer while Gram-negative bacteria have a thin peptidoglycan layer but a thick lipopolysaccharide layer (Pasquina-Lemonche et al., 2020). A similar reason was also given by several other investigators for the antimicrobial activity of the synthesized AgNPs (Kalpana and Lee, 2013). Investigators reported that spherical AgNPs have higher antibacterial/antimicrobial activity due to high SVR (Al-Ogaidi and Rasheed, 2022). Moreover, due to their large surface area, they could bind with various ligands. Smaller AgNPs can move more deeper into the microbial cells through the cell membrane and there is enhanced

antimicrobial activity with the reduction in the AgNPs size (Anees Ahmad et al., 2020; Wypij et al., 2021). AgNPs get attached to the cell membrane where it releases Ag ions slowly. Further, AgNPs are reported to develop pits in the cell wall of microorganisms which leads to enhances permeability and leakage of cellular components through the plasma membrane (Tripathi et al., 2017; Matras et al., 2022).

5. Conclusions

The silver nanoparticle of different shapes and sizes could be synthesized by using different bacterial strains which have different types of microbial proteins and enzymes. The variations in the microbial proteins and enzymes help in determining the morphology of the silver nanoparticles. The microscopic techniques confirm the spherical shape of AgNPs, while EDS shows the purity of the AgNPs. The XRD exhibited the crystalline nature of the AgNPs, while FTIR showed the typical IR bands for the AgNPs. FTIR also showed the presence of organic biomolecules with the synthesized AgNPs. The methyl orange dye removal percentage for the AgNPs was highest up to 20% with AgNPs-M. While the highest antibacterial activity was exhibited with AgNPs-M against *B. megaterium* i.e., 12 mm.

References

- Al-Ogaidi, M. A. Z., and Rasheed, B. G. (2022). Enhancement of Antimicrobial Activity of Silver Nanoparticles Using Lasers. *Lasers in Manufacturing and Materials Processing* 9, 610–621. doi: 10.1007/s40516-022-00192-4.
- Al-Tohamy, R., Ali, S. S., Li, F., Okasha, K. M., Mahmoud, Y. A.-G., Elsamahy, T., et al. (2022). A critical review on the treatment of dye-containing wastewater: Ecotoxicological and health

concerns of textile dyes and possible remediation approaches for environmental safety.

Ecotoxicol Environ Saf 231, 113160. doi: <https://doi.org/10.1016/j.ecoenv.2021.113160>.

Amari, A., Yadav, V. K., Pathan, S. K., Singh, B., Osman, H., Choudhary, N., et al. (2023).

Remediation of Methyl Red Dye from Aqueous Solutions by Using Biosorbents Developed

from Floral Waste. *Adsorption Science & Technology* 2023, 1–17. doi:

10.1155/2023/1532660.

Anees Ahmad, S., Sachi Das, S., Khatoon, A., Tahir Ansari, M., Afzal, Mohd., Saquib Hasnain,

M., et al. (2020). Bactericidal activity of silver nanoparticles: A mechanistic review. *Mater*

Sci Energy Technol 3, 756–769. doi: <https://doi.org/10.1016/j.mset.2020.09.002>.

Austin, W., Granger, S., Felicia, R., P, P. L., E, F. D., G, F. V., et al. (2020). Newly Named

Klebsiella aerogenes (formerly Enterobacter aerogenes) Is Associated with Poor Clinical

Outcomes Relative to Other Enterobacter Species in Patients with Bloodstream Infection. *J*

Clin Microbiol 58, 10.1128/jcm.00582-20. doi: 10.1128/jcm.00582-20.

Ballén, V., Gabasa, Y., Ratia, C., Ortega, R., Tejero, M., and Soto, S. (2021). Antibiotic Resistance

and Virulence Profiles of Klebsiella pneumoniae Strains Isolated From Different Clinical

Sources. *Front Cell Infect Microbiol* 11. Available at:

<https://www.frontiersin.org/articles/10.3389/fcimb.2021.738223>.

Betts, H. D., Whitehead, C., and Harris, H. H. (2021). Silver in biology and medicine: opportunities

for metallomics researchers. *Metallomics* 13, mfaa001. doi: 10.1093/mtomcs/mfaa001.

Bouafia, A., Laouini, S. E., Ahmed, A. S. A., Soldatov, A. V., Algarni, H., Chong, K. F., et al.

(2021). The recent progress on silver nanoparticles: Synthesis and electronic applications.

Nanomaterials 11. doi: 10.3390/nano11092318.

- Carter, E. L., Boer, J. L., Farrugia, M. A., Flugga, N., Towns, C. L., and Hausinger, R. P. (2011). Function of UreB in *Klebsiella aerogenes* Urease. *Biochemistry* 50, 9296–9308. doi: 10.1021/bi2011064.
- Cekuolyte, K., Gudiukaite, R., Klimkevicius, V., Mazrimaite, V., Maneikis, A., and Lastauskiene, E. (2023). Biosynthesis of Silver Nanoparticles Produced Using *Geobacillus* spp. *Bacteria. Nanomaterials* 13. doi: 10.3390/nano13040702.
- Chahar, M., Khaturia, S., Singh, H. L., Singh Solanki, V., Agarwal, N., Sahoo, K., et al. (2023). Recent advances in the effective removal of hazardous pollutants from wastewater by using nanomaterials-A review. *Front. Environ. Sci.* 11. doi: 10.3389/fenvs.2023.1226101.
- Choudhary, N., Dhingra, N., Gacem, A., Yadav, V. K., Verma, R. K., Choudhary, M., et al. (2023). Towards further understanding the applications of endophytes: enriched source of bioactive compounds and bio factories for nanoparticles. *Front Plant Sci* 14. doi: 10.3389/fpls.2023.1193573.
- Dalvand, R., Kianpour, E., Tahzibi, H., and Azizian, S. (2020). MgO nano-sheets for adsorption of anionic dyes from aqueous solution: Equilibrium and kinetics studies. *Surfaces and Interfaces* 21, 100722. doi: <https://doi.org/10.1016/j.surfin.2020.100722>.
- Das, A., and Mishra, S. (2017). Removal of textile dye reactive green-19 using bacterial consortium: Process optimization using response surface methodology and kinetics study. *J Environ Chem Eng* 5, 612–627. doi: <https://doi.org/10.1016/j.jece.2016.10.005>.
- Dash, S., Chaudhuri, H., Gupta, R., and Nair, U. G. (2018). Adsorption study of modified coal fly ash with sulfonic acid as a potential adsorbent for the removal of toxic reactive dyes from

- aqueous solution: Kinetics and thermodynamics. *J Environ Chem Eng* 6, 5897–5905. doi:
<https://doi.org/10.1016/j.jece.2018.05.017>.
- Degefa, A., Bekele, B., Jule, L. T., Fikadu, B., Ramaswamy, S., Dwarampudi, L. P., et al. (2021).
Green Synthesis, Characterization of Zinc Oxide Nanoparticles, and Examination of
Properties for Dye-Sensitive Solar Cells Using Various Vegetable Extracts. *J Nanomater*
2021. doi: 10.1155/2021/3941923.
- Esmail, R., Afshar, A., Morteza, M., Abolfazl, A., and Akhondi, E. (2022). Synthesis of silver
nanoparticles with high efficiency and stability by culture supernatant of *Bacillus ROM6*
isolated from Zarshouran gold mine and evaluating its antibacterial effects. *BMC Microbiol*
22. doi: 10.1186/s12866-022-02490-5.
- Giri, A. K., Jena, B., Biswal, B., Pradhan, A. K., Arakha, M., Acharya, S., et al. (2022). Green
synthesis and characterization of silver nanoparticles using *Eugenia roxburghii* DC. extract
and activity against biofilm-producing bacteria. *Sci Rep* 12, 8383. doi: 10.1038/s41598-022-
12484-y.
- Gurunathan, S. (2019). Rapid biological synthesis of silver nanoparticles and their enhanced
antibacterial effects against *Escherichia fergusonii* and *Streptococcus mutans*. *Arabian*
Journal of Chemistry 12, 168–180. doi: <https://doi.org/10.1016/j.arabjc.2014.11.014>.
- Hamouda, R. A., Hussein, M. H., Abo-elmagd, R. A., and Bawazir, S. S. (2019). Synthesis and
biological characterization of silver nanoparticles derived from the cyanobacterium
Oscillatoria limnetica. *Sci Rep* 9, 13071. doi: 10.1038/s41598-019-49444-y.
- Harja, M., Buema, G., and Bucur, D. (2022). Recent advances in removal of Congo Red dye by
adsorption using an industrial waste. *Sci Rep* 12, 6087. doi: 10.1038/s41598-022-10093-3.

- I, T. W., and David, A. (1972). Catalase Test as an Aid to the Identification of Enterobacteriaceae. *Appl Microbiol* 24, 58–61. doi: 10.1128/am.24.1.58-61.1972.
- Ibrahim, E., Fouad, H., Zhang, M., Zhang, Y., Qiu, W., Yan, C., et al. (2019). Biosynthesis of silver nanoparticles using endophytic bacteria and their role in inhibition of rice pathogenic bacteria and plant growth promotion. *RSC Adv* 9, 29293–29299. doi: 10.1039/c9ra04246f.
- Imoisili, P. E., Nwanna, E. C., and Jen, T.-C. (2022). Facile Preparation and Characterization of Silica Nanoparticles from South Africa Fly Ash Using a Sol–Gel Hydrothermal Method. *Processes* 10, 2440. doi: 10.3390/pr10112440.
- Javaid, A., Oloketuyi, S. F., Khan, M. M., and Khan, F. (2018). Diversity of Bacterial Synthesis of Silver Nanoparticles. *Bionanoscience* 8, 43–59. doi: 10.1007/s12668-017-0496-x.
- Jubeh, B., Breijyeh, Z., and Karaman, R. (2020). Resistance of gram-positive bacteria to current antibacterial agents and overcoming approaches. *Molecules* 25. doi: 10.3390/molecules25122888.
- Kalpana, D., and Lee, Y. S. (2013). Synthesis and characterization of bactericidal silver nanoparticles using cultural filtrate of simulated microgravity grown *Klebsiella pneumoniae*. *Enzyme Microb Technol* 52, 151–156. doi: 10.1016/j.enzmictec.2012.12.006.
- Kalwar, K., and Shan, D. (2018). Antimicrobial effect of silver nanoparticles (AgNPs) and their mechanism – a mini review. *Micro Nano Lett* 13, 277–280. doi: <https://doi.org/10.1049/mnl.2017.0648>.

- Karami-Zarandi, M., Rahdar, H. A., Esmaeili, H., and Ranjbar, R. (2023). *Klebsiella pneumoniae*: an update on antibiotic resistance mechanisms. *Future Microbiol* 18, 65–81. doi: 10.2217/fmb-2022-0097.
- Karunakaran, G., Jagathambal, M., Gusev, A., Torres, J. A. L., Kolesnikov, E., and Kuznetsov, D. (2017). Rapid Biosynthesis of AgNPs Using Soil Bacterium *Azotobacter vinelandii* With Promising Antioxidant and Antibacterial Activities for Biomedical Applications. *JOM* 69, 1206–1212. doi: 10.1007/s11837-016-2175-8.
- Kumar, N., and Dubey, R. C. (2022). Biosynthesis of silver nanoparticles using the endophyte *Enterobacter roggenkampii* BLS02 from *Barleria lupulina* and their role in the inhibition of food borne bacteria. *Vegetos*. doi: 10.1007/s42535-022-00514-z.
- Kyung, J. W., Cheong, K. H., Woo, K. K., Sook, S., Hyun, K. S., and Ho, P. Y. (2008). Antibacterial Activity and Mechanism of Action of the Silver Ion in *Staphylococcus aureus* and *Escherichia coli*. *Appl Environ Microbiol* 74, 2171–2178. doi: 10.1128/AEM.02001-07.
- Matras, E., Gorczyca, A., Przemieniecki, S. W., and Oćwieja, M. (2022). Surface properties-dependent antifungal activity of silver nanoparticles. *Sci Rep* 12, 18046. doi: 10.1038/s41598-022-22659-2.
- Merciecca, T., Bornes, S., Nakusi, L., Theil, S., Rendueles, O., Forestier, C., et al. (2022). Role of *Klebsiella pneumoniae* Type VI secretion system (T6SS) in long-term gastrointestinal colonization. *Sci Rep* 12, 16968. doi: 10.1038/s41598-022-21396-w.
- Modi, S., Yadav, V. K., Amari, A., Osman, H., Igwegbe, C. A., and Fulekar, M. H. (2023). Nanobioremediation: a bacterial consortium-zinc oxide nanoparticle-based approach for the

- removal of methylene blue dye from wastewater. *Environmental Science and Pollution Research* 30, 72641–72651. doi: 10.1007/s11356-023-27507-y.
- Murukutti, M. K., and Jena, H. (2022). Synthesis of nano-crystalline zeolite-A and zeolite-X from Indian coal fly ash, its characterization and performance evaluation for the removal of Cs⁺ and Sr²⁺ from simulated nuclear waste. *J Hazard Mater* 423, 127085. doi: <https://doi.org/10.1016/j.jhazmat.2021.127085>.
- Naganthran, A., Verasoundarapandian, G., Khalid, F. E., Masarudin, M. J., Zulkharnain, A., Nawawi, N. M., et al. (2022). Synthesis, Characterization and Biomedical Application of Silver Nanoparticles. *Materials* 15. doi: 10.3390/ma15020427.
- Nisha, C., Bhawana, P., and Fulekar, M. H. (2017). Antimicrobial Potential of Green Synthesized Silver nanoparticles using *Sida acuta* Leaf extract. Available at: www.tsijournals.com.
- Pan, S., Yao, T., Du, L., and Wei, Y. (2020). Site-saturation mutagenesis at amino acid 329 of *Klebsiella pneumoniae* halophilic α -amylase affects enzymatic properties. *J Biosci Bioeng* 129, 155–159. doi: <https://doi.org/10.1016/j.jbiosc.2019.09.002>.
- Pasquina-Lemonche, L., Burns, J., Turner, R. D., Kumar, S., Tank, R., Mullin, N., et al. (2020). The architecture of the Gram-positive bacterial cell wall. *Nature* 582, 294–297. doi: 10.1038/s41586-020-2236-6.
- Patel, H., Yadav, V. K., Yadav, K. K., Choudhary, N., Kalasariya, H., Alam, M. M., et al. (2022). A Recent and Systemic Approach towards Microbial Biodegradation of Dyes from Textile Industries. 14, 3163. doi: 10.3390/w14193163.

- Peiris, M. M. K., Fernando, S. S. N., Jayaweera, P. M., Arachchi, N. D. H., and Guansekara, T. D. C. P. (2018). Comparison of Antimicrobial Properties of Silver Nanoparticles Synthesized from Selected Bacteria. *Indian J Microbiol* 58, 301–311. doi: 10.1007/s12088-018-0723-3.
- Raza, S., Ansari, A., Siddiqui, N. N., Ibrahim, F., Abro, M. I., and Aman, A. (2021). Biosynthesis of silver nanoparticles for the fabrication of non cytotoxic and antibacterial metallic polymer based nanocomposite system. *Sci Rep* 11, 10500. doi: 10.1038/s41598-021-90016-w.
- Robati, D., Mirza, B., Rajabi, M., Moradi, O., Tyagi, I., Agarwal, S., et al. (2016). Removal of hazardous dyes-BR 12 and methyl orange using graphene oxide as an adsorbent from aqueous phase. *Chemical Engineering Journal* 284, 687–697. doi: <https://doi.org/10.1016/j.cej.2015.08.131>.
- Saeed, S., Iqbal, A., and Ashraf, M. A. (2020). Bacterial-mediated synthesis of silver nanoparticles and their significant effect against pathogens. *Environmental Science and Pollution Research* 27, 37347–37356. doi: 10.1007/s11356-020-07610-0.
- Saleh, M. N., and Khoman Alwan, S. (2020). Bio-synthesis of silver nanoparticles from bacteria *Klebsiella pneumonia*: Their characterization and antibacterial studies. in *Journal of Physics: Conference Series* (IOP Publishing Ltd). doi: 10.1088/1742-6596/1664/1/012115.
- Sayyid, N. H., and Zghair, Z. R. (2021). Biosynthesis of silver nanoparticles produced by *Klebsiella pneumoniae*. *Mater Today Proc* 42, 2045–2049. doi: <https://doi.org/10.1016/j.matpr.2020.12.257>.
- Singh, P., and Mijakovic, I. (2022). Strong Antimicrobial Activity of Silver Nanoparticles Obtained by the Green Synthesis in *Viridibacillus* sp. Extracts. *Front Microbiol* 13. Available at: <https://www.frontiersin.org/articles/10.3389/fmicb.2022.820048>.

- Soltani, S., Gacem, A., Choudhary, N., Yadav, V. K., Alsaeedi, H., Modi, S., et al. (2023). Scallion Peel Mediated Synthesis of Zinc Oxide Nanoparticles and Their Applications as Nano fertilizer and Photocatalyst for Removal of Organic Pollutants from Wastewater. *Water (Switzerland)* 15. doi: 10.3390/w15091672.
- Srinivasan, R., Mathivanan, K., Govindarajan, R. K., Uthaya Chandirika, J., and Govindasamy, C. (2022). Extracellular synthesis of silver nanoparticles by bioluminescent bacteria: characterization and evaluation of its antibacterial and antioxidant properties. *Int Nano Lett* 12, 169–177. doi: 10.1007/s40089-021-00360-y.
- Tarekegn, M. M., Balakrishnan, R. M., Hiruy, A. M., and Dekebo, A. H. (2021). Removal of methylene blue dye using nano zerovalent iron, nanoclay and iron impregnated nanoclay – a comparative study. *RSC Adv* 11, 30109–30131. doi: 10.1039/D1RA03918K.
- Terzioğlu, E., Arslan, M., Balaban, B. G., and Çakar, Z. P. (2022). Microbial silver resistance mechanisms: recent developments. *World J Microbiol Biotechnol* 38, 158. doi: 10.1007/s11274-022-03341-1.
- Tripathi, D. K., Tripathi, A., Shweta, Singh, S., Singh, Y., Vishwakarma, K., et al. (2017). Uptake, Accumulation and Toxicity of Silver Nanoparticle in Autotrophic Plants, and Heterotrophic Microbes: A Concentric Review. *Front Microbiol* 8. Available at: <https://www.frontiersin.org/articles/10.3389/fmicb.2017.00007>.
- Vimalanathan, A. B., Ernest, V., Arumugasamy, K., and Tyagi, M. G. (2013). Biosynthesis of silver nano-particles by the bacterium *Micrococcus luteus*. *Int J Appl Biol Pharm* 4, 77–83. Available at: www.ijabpt.com.

- Wintachai, P., Naknaen, A., Thammaphet, J., Pomwised, R., Phaonakrop, N., Roytrakul, S., et al. (2020). Characterization of extended-spectrum- β -lactamase producing *Klebsiella pneumoniae* phage KP1801 and evaluation of therapeutic efficacy in vitro and in vivo. *Sci Rep* 10, 11803. doi: 10.1038/s41598-020-68702-y.
- Wypij, M., Jędrzejewski, T., Trzcińska-Wencel, J., Ostrowski, M., Rai, M., and Golińska, P. (2021). Green Synthesized Silver Nanoparticles: Antibacterial and Anticancer Activities, Biocompatibility, and Analyses of Surface-Attached Proteins. *Front Microbiol* 12. Available at: <https://www.frontiersin.org/articles/10.3389/fmicb.2021.632505>.
- Yadav, M., Dwibedi, V., Sharma, S., and George, N. (2022a). Biogenic silica nanoparticles from agro-waste: Properties, mechanism of extraction and applications in environmental sustainability. *J Environ Chem Eng* 10, 108550. doi: <https://doi.org/10.1016/j.jece.2022.108550>.
- Yadav, V. K., Amari, A., Gacem, A., Elboughdiri, N., Eltayeb, L. B., and Fulekar, M. H. (2023a). Treatment of Fly-Ash-Contaminated Wastewater Loaded with Heavy Metals by Using Fly-Ash-Synthesized Iron Oxide Nanoparticles. *Water (Basel)* 15, 908. doi: 10.3390/w15050908.
- Yadav, V. K., Amari, A., Wanale, S. G., Osman, H., and Fulekar, M. H. (2023b). Synthesis of Floral-Shaped Nanosilica from Coal Fly Ash and Its Application for the Remediation of Heavy Metals from Fly Ash Aqueous Solutions. *Sustainability* 15, 2612. doi: 10.3390/su15032612.
- Yadav, V. K., Gnanamoorthy, G., Ali, D., Bera, S. P., Roy, A., Kumar, G., et al. (2022b). Cytotoxicity, Removal of Congo Red Dye in Aqueous Solution Using Synthesized

Amorphous Iron Oxide Nanoparticles from Incense Sticks Ash Waste. *J Nanomater* 2022.
doi: 10.1155/2022/5949595.

Yadav, V. K., Inwati, G. K., Ali, D., Gnanamoorthy, G., Bera, S. P., Khan, S. H., et al. (2022c).
Remediation of Azure A Dye from Aqueous Solution by Using Surface-Modified Coal Fly
Ash Extracted Ferrospheres by Mineral Acids and Toxicity Assessment. *Adsorption Science
and Technology* 2022. doi: 10.1155/2022/7012889.

Yang, J., Shojaei, S., and Shojaei, S. (2022). Removal of drug and dye from aqueous solutions by
graphene oxide: Adsorption studies and chemometrics methods. *NPJ Clean Water* 5, 5. doi:
10.1038/s41545-022-00148-3.

Yassin, M. T., Mostafa, A. A. F., Al-Askar, A. A., and Al-Otibi, F. O. (2022). Synergistic
Antibacterial Activity of Green Synthesized Silver Nanomaterials with Colistin Antibiotic
against Multidrug-Resistant Bacterial Pathogens. *Crystals (Basel)* 12. doi:
10.3390/cryst12081057.

Figure 1

Figure 1

FIGURE 1 Schematic diagram for the synthesis of AgNPs using bacterial supernatant.

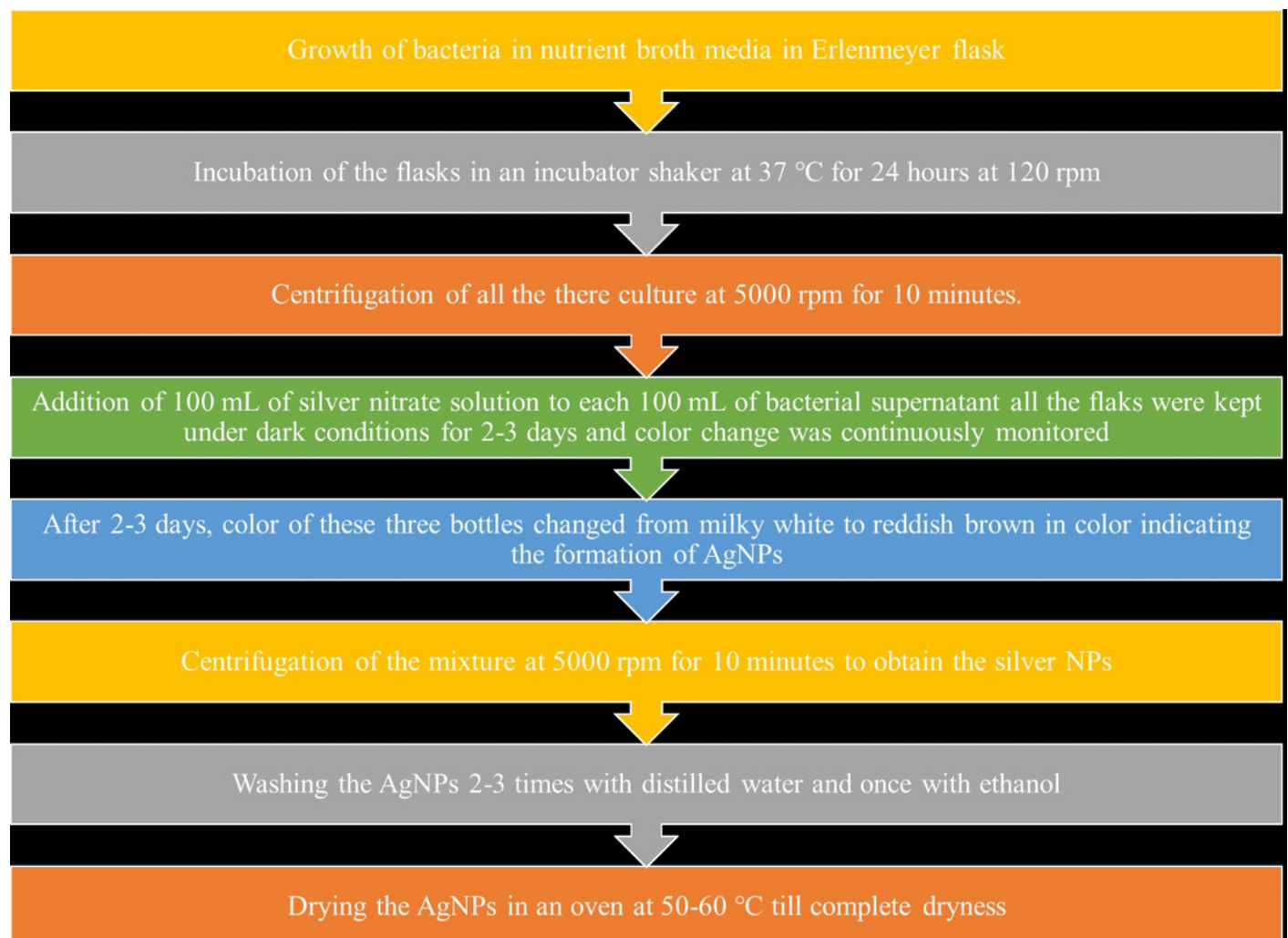


Figure 2

Figure 2

FIGURE 2 Schematic diagram for the formation of AgNPs from silver ions by bacteria via NADH-dependent nitrate reductase enzyme.

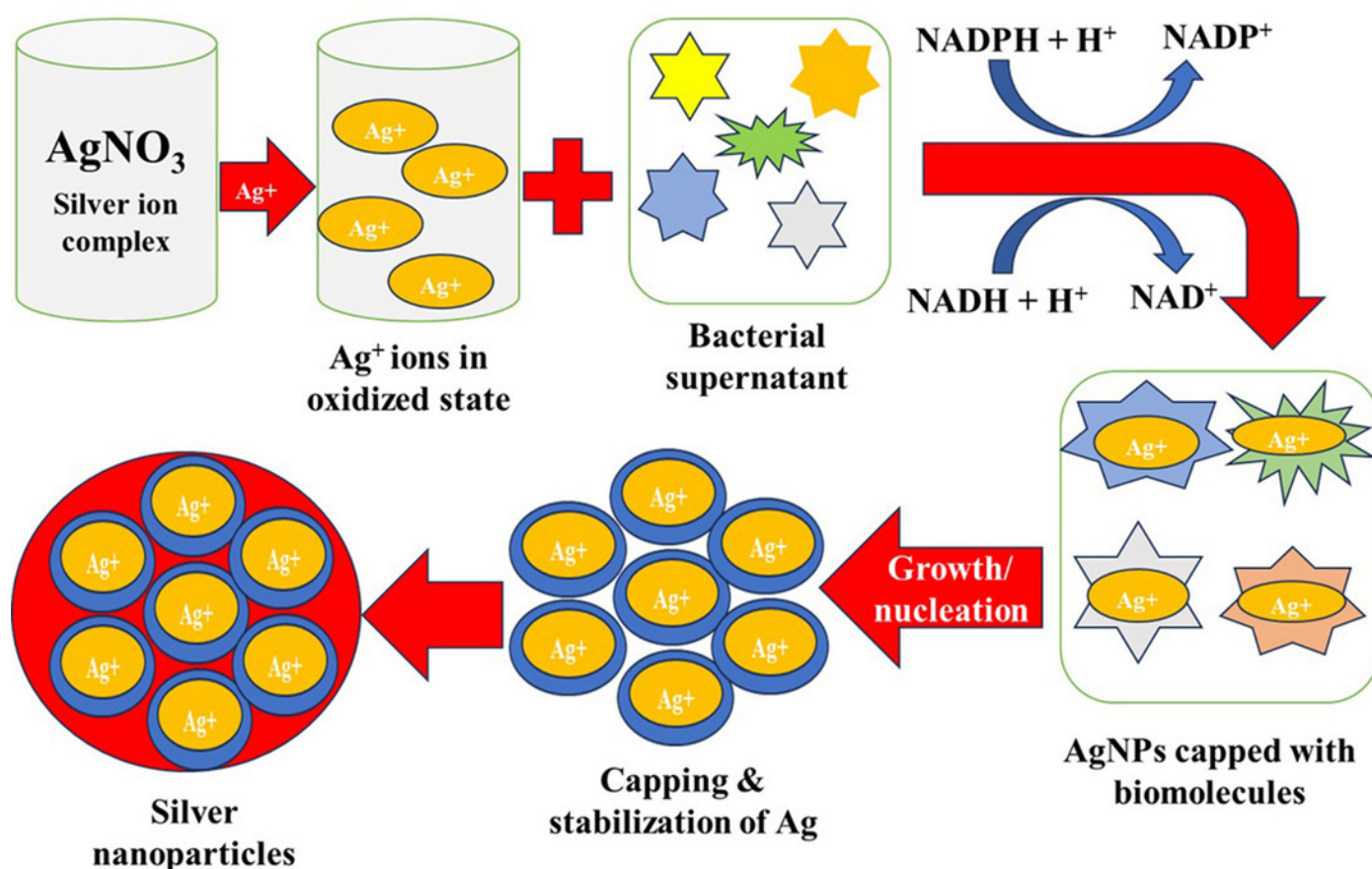


Figure 3

Figure 3

FIGURE 3 UV-Vis measurement of AgNPs synthesized by bacteria.

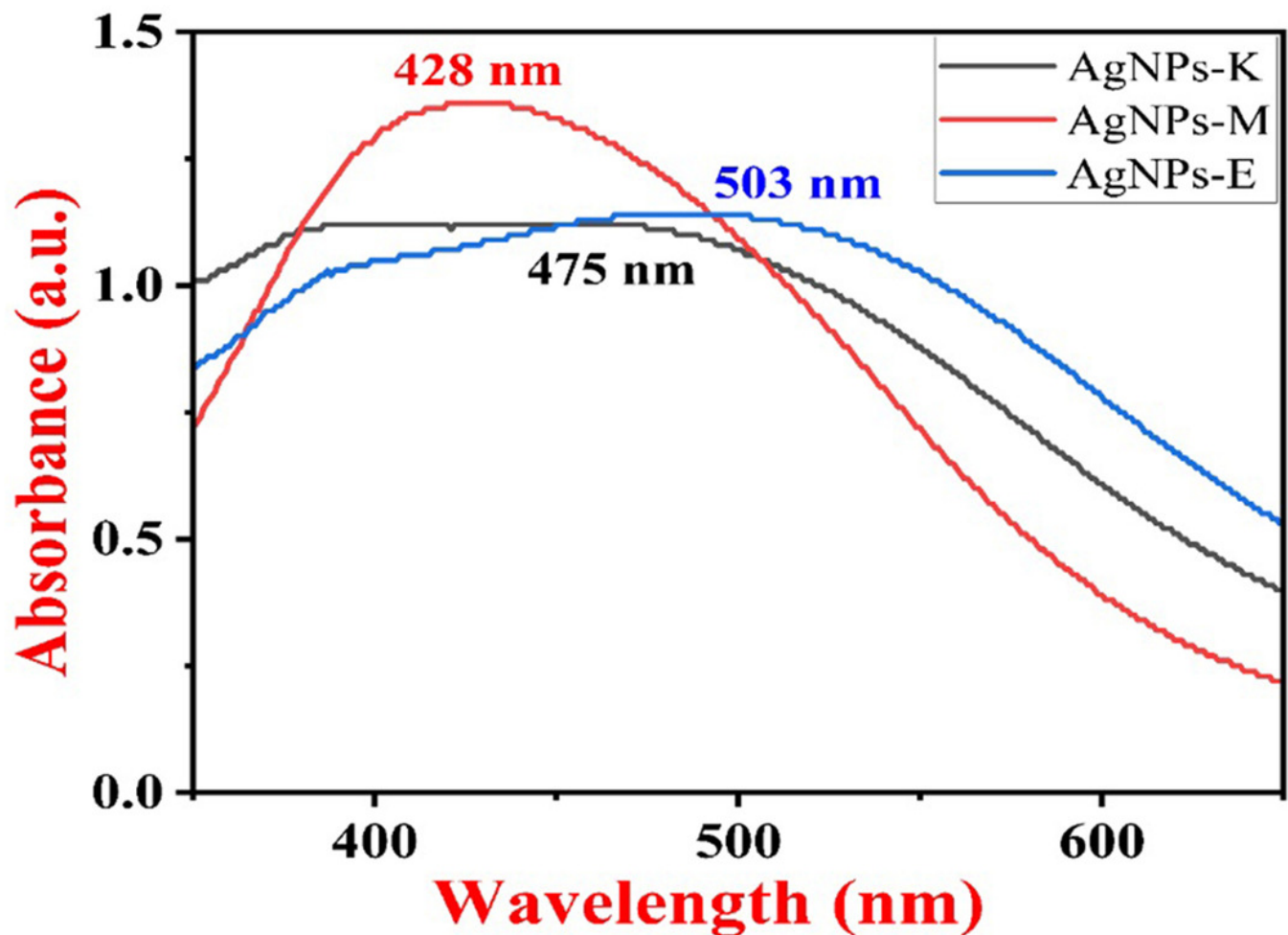


Figure 4

Figure 4

FIGURE 4 FTIR spectra of AgNPs synthesized by bacteria.

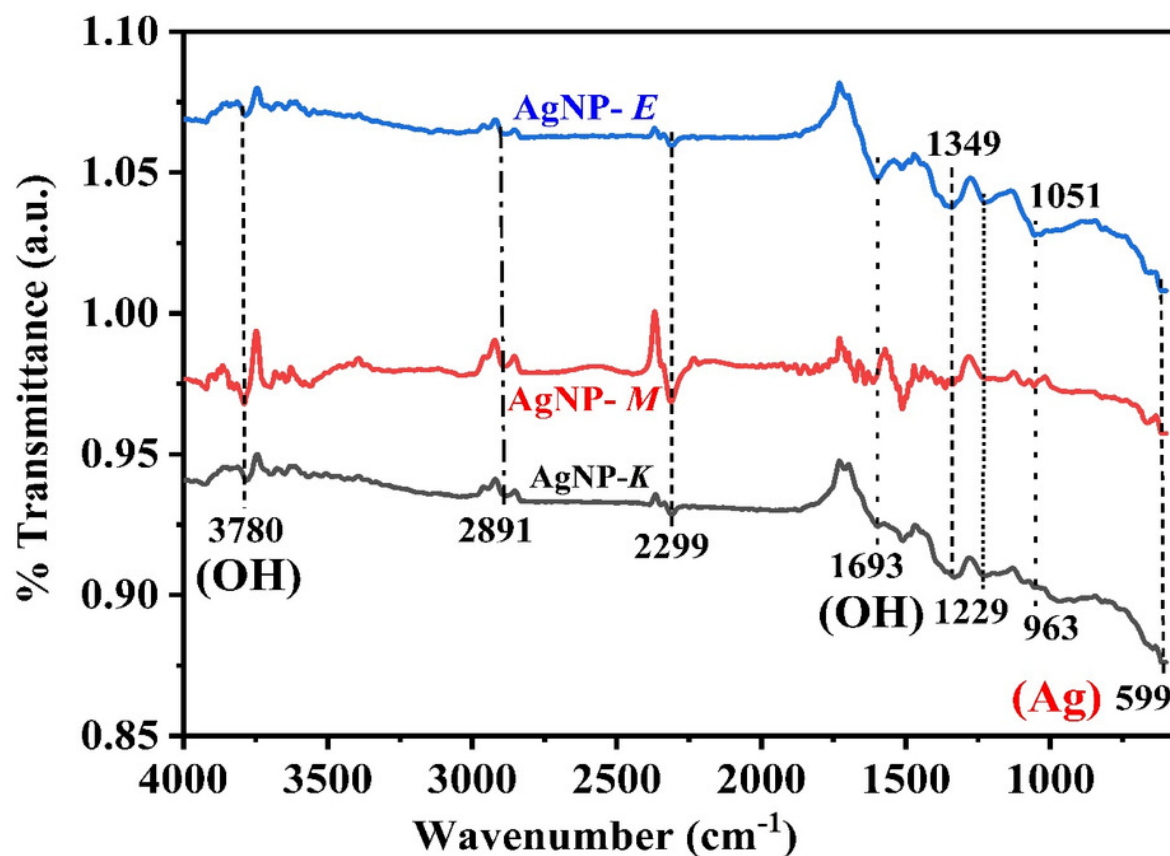


Figure 5

Figure 5

FIGURE 5 XRD pattern of silver nanoparticles synthesized by bacteria.

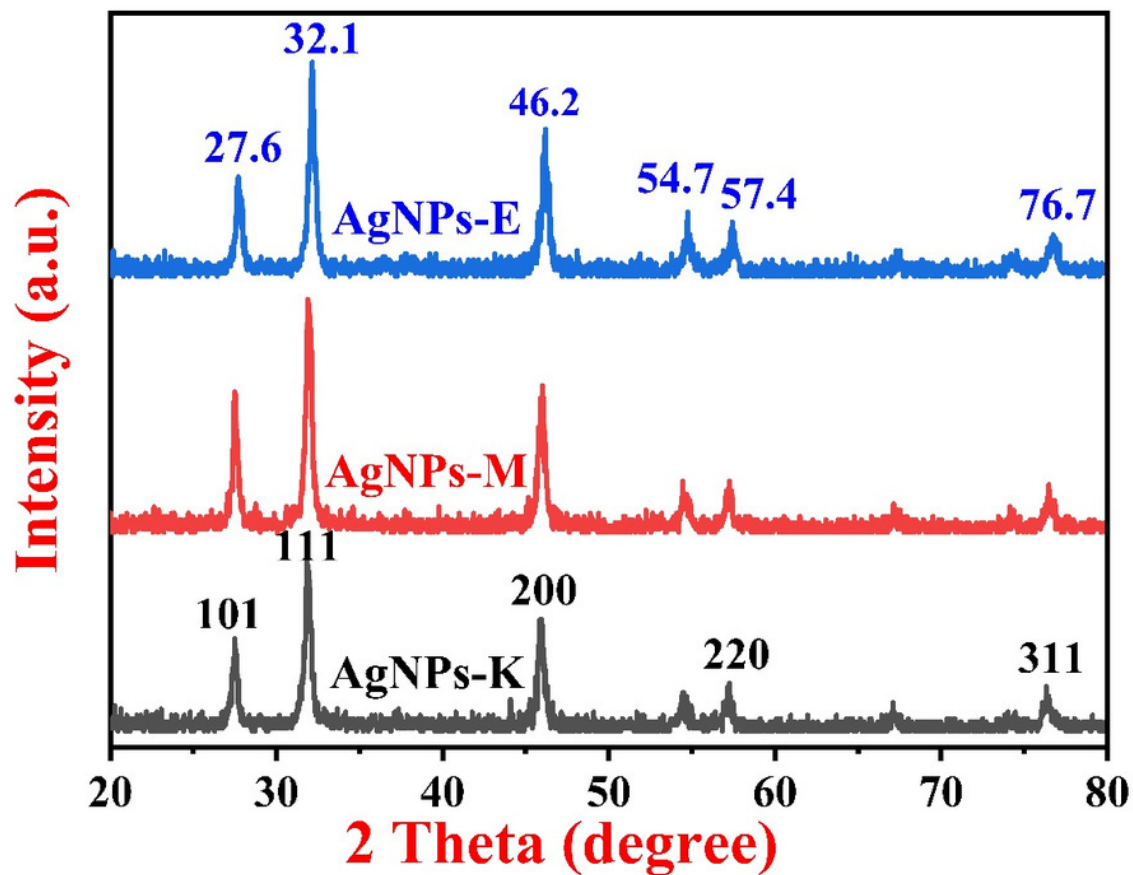


Figure 6

Figure 6

FIGURE 6 FESEM images (a-f), EDS spot (g), and EDS spectra and elemental table (h) for AgNPs-K. FESEM images (i-l), EDS spot (m) and EDS spectra, and elemental table (n) for AgNPs-M. FESEM images (o-r), EDS spot (s) and EDS spectra, and elemental table (t) for AgNPs-E.

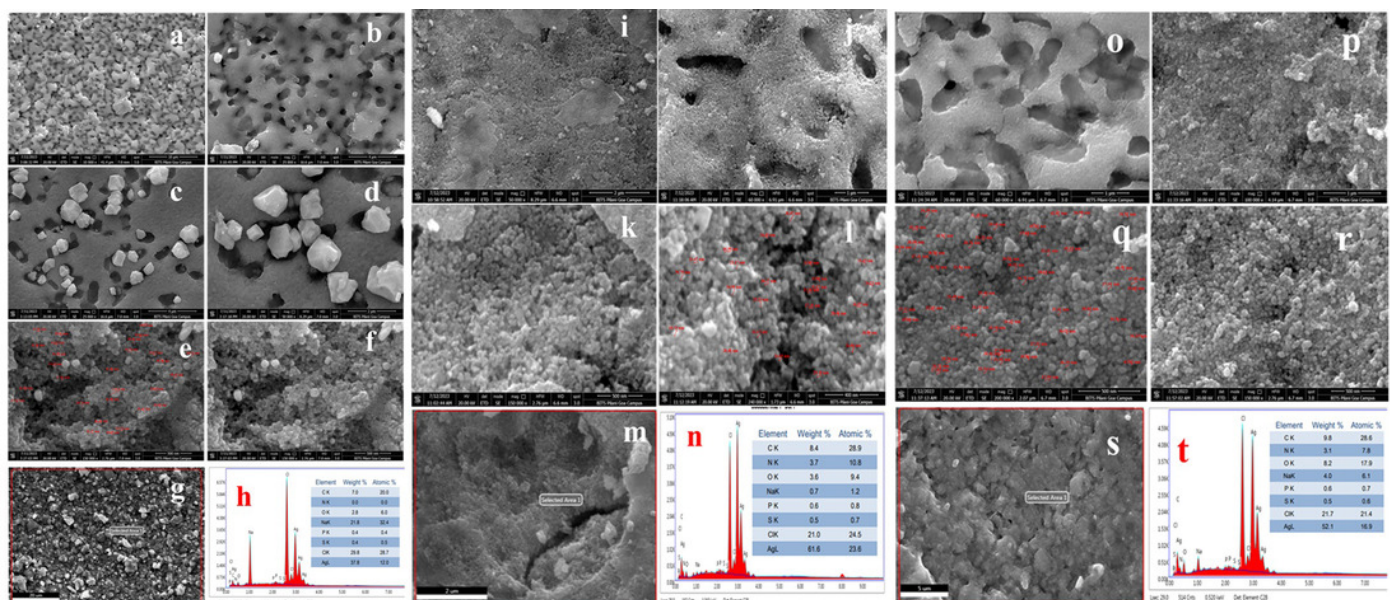


Figure 7

Figure 7

FIGURE 7 MO dye removal by different types of AgNPs with respect to contact time as measured by UV-Vis spectrophotometer.

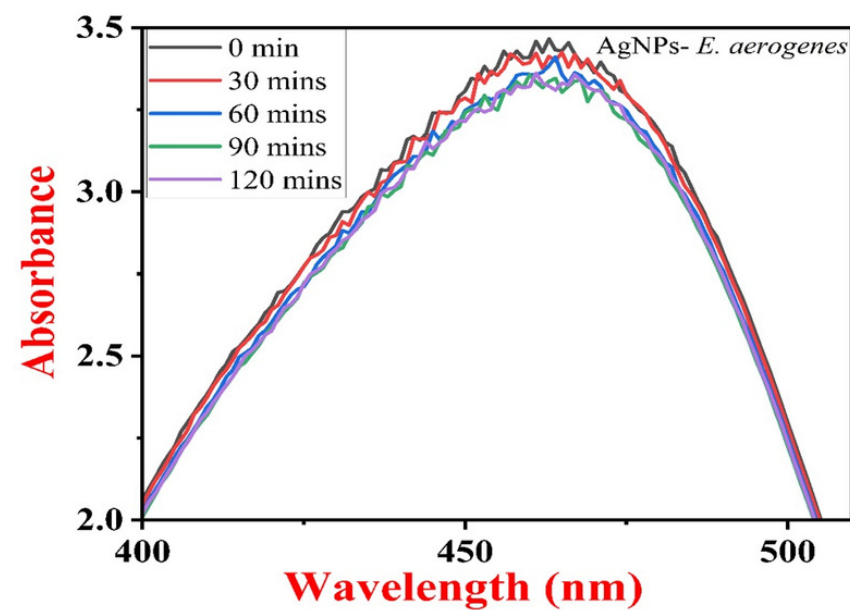
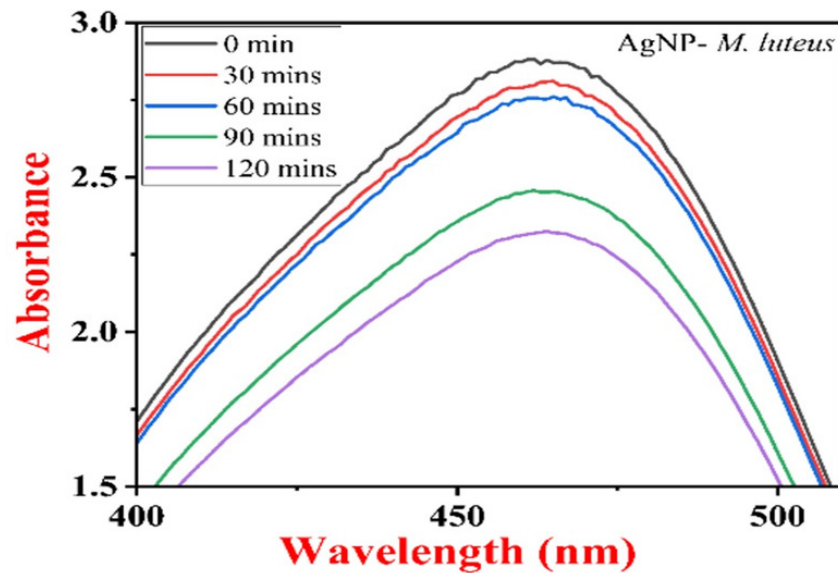
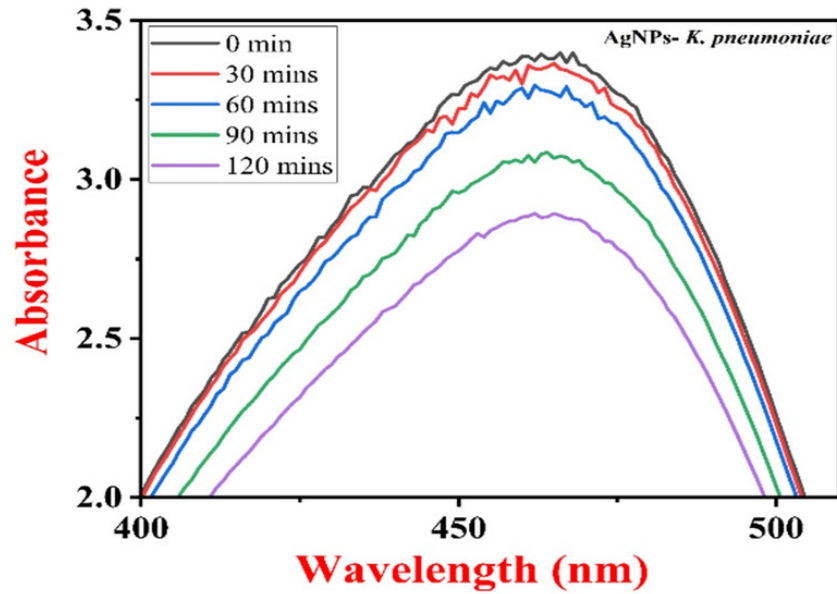


Figure 8

Figure 8

FIGURE 8 Percentage removal of MO dye by all three types of AgNPs.

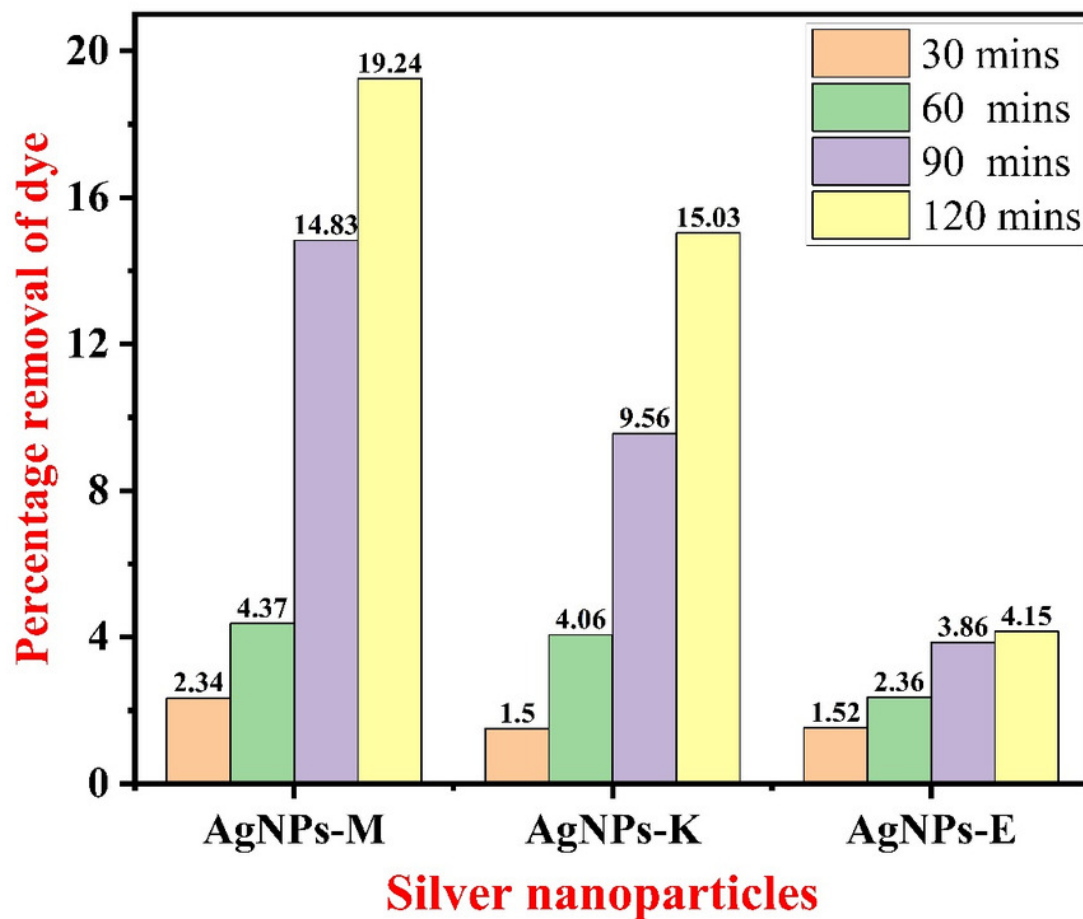


Figure 9

Figure 9

FIGURE 9 Antibacterial activity, zone of inhibition of AgNPs synthesized against the tested bacterial species.

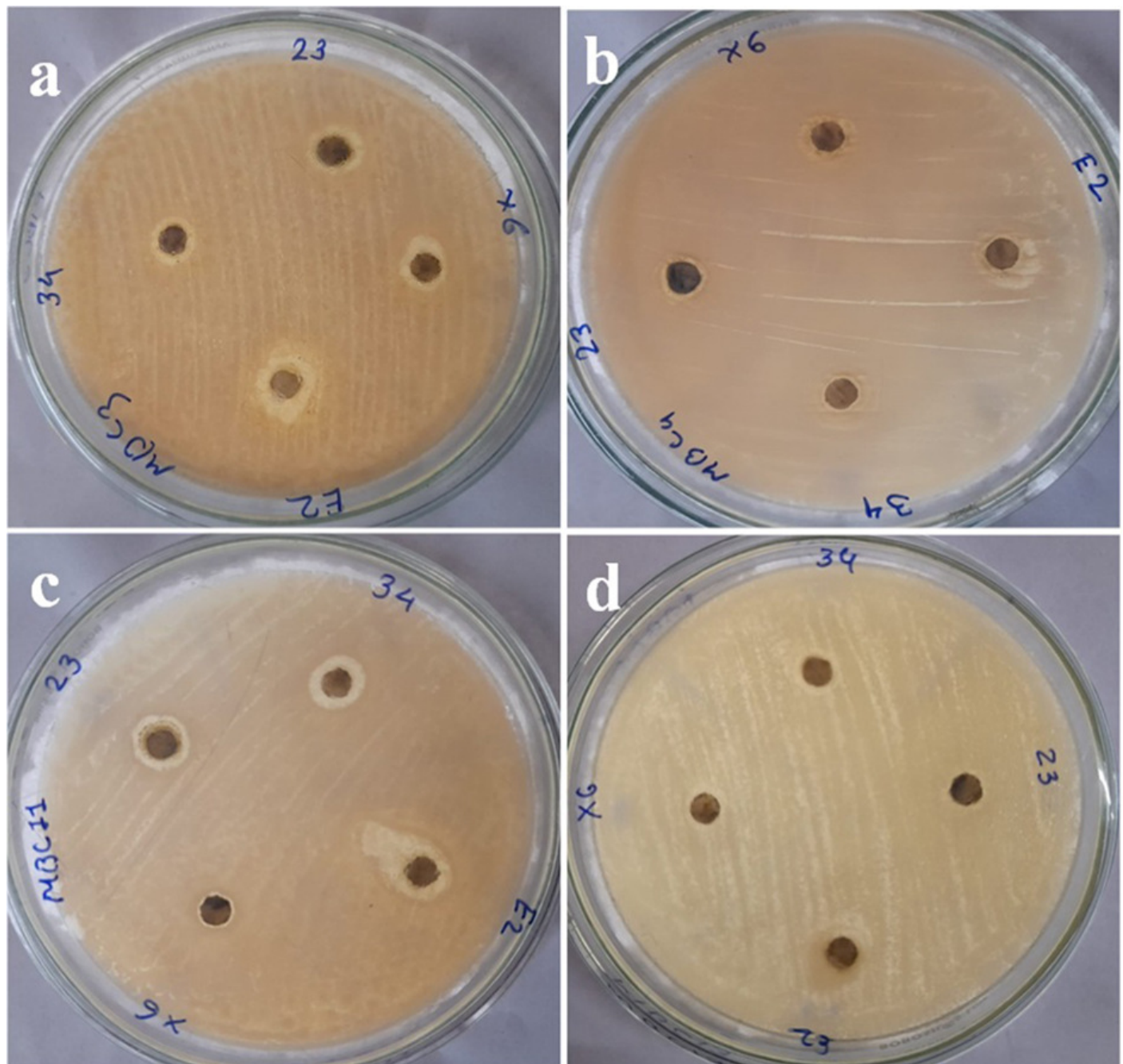


Table 1 (on next page)

Table 1

TABLE 1 The major microbial proteins and enzymes present in *K. pneumoniae*, *M. luteus*, and *E. aerogenes*.

1 **TABLE 1** The major microbial proteins and enzymes present in *K. pneumoniae*, *M. luteus*,
2 and *E. aerogenes*.

Various microbial proteins and enzymes			
<i>K. pneumoniae</i>	<i>M. luteus</i>	<i>E. aerogenes</i>	References
<i>α-Lactamase</i>	Esterase	<i>α-Lactamase</i>	(Wintachai et al., 2020; Karami-Zarandi et al., 2023)
<i>Lipases</i>	Proteases	<i>Lipases</i>	(Merciecca et al., 2022)
<i>Proteases</i>	Phytases	<i>Proteases</i>	(Wintachai et al., 2020)
<i>Amylases</i>	Dehydrogenases	<i>Amylases</i>	(Pan et al., 2020)
<i>Catalase</i>	Lipases	<i>Catalase</i>	(I and David, 1972)
<i>Gelatinase</i>	-	<i>Gelatinase</i>	(Austin et al., 2020)
<i>Urease</i>	-	<i>Urease</i>	(Carter et al., 2011)

3

Table 2 (on next page)

Table 2

TABLE 2 Comparison between all the elements present in all three types of AgNPs.

1 **TABLE 2 Comparison between all the elements present in all three types of AgNPs.**

Elements (At. wt.%)	AgNPs- <i>M. luteus</i>	AgNPs- <i>K. pneumoniae</i>	AgNPs- <i>E. aerogenes</i>
Ag	61.6	37.8	52.1
Cl	21.0	29.8	21.7
O	3.6	2.8	8.2
C	8.4	7.0	9.8
Na	0.7	21.8	4.0
N	3.7	0.0	3.1
P	0.6	0.4	0.6
S	0.5	0.4	0.5

2

Table 3(on next page)

Table 3

TABLE 3 The comparative analysis of the bacterially synthesized AgNPs.

1 TABLE 3 The comparative analysis of the bacterially synthesized AgNPs.

Microorganism	Particle size (nm)	Elements observed	Morphology	XRD peaks and size	Absorbance maxima wavelength (nm)	FTIR bands	References
<i>K. pneumoniae</i>	40.47±89		Cube-shape, irregular heterogeneous forms	-	-	-	(Sayyid and Zghair, 2021)
<i>Pseudomonas aeruginosa</i> ATCC 27853	11.71±2.73	-	Spherical	-	427	1643, 1586, 1397 and 1042 cm ⁻¹	(Peiris et al., 2018)
<i>S. aureus</i> ATCC 25923	11.14±6.59	-		--	430	2164.86, 2049.17 and 1979.69 cm ⁻¹	
<i>E. coli</i>	13-16	-			420–	2916.88 cm ⁻¹	

ATCC 25922					435		
<i>Acinetobacter baumannii</i>	8-12	-		-	420–435	1643.75, 2161.48, and 2924.28 cm ⁻¹	
<i>K. pneumoniae</i>	5 & 50 (TEM)	-	Spherical, & triangular (small amount)	37.76°, 45.87°, 64.08° and 77.11° for e (1 1 1), (2 0 0), (2 2 0) and (3 1 1)	405–407	2964.55, 1262.22, 1095.89, 1021.96, 800.73, 2960.64, 1650.01, 865.33, 701, 477.07 cm ⁻¹	(Kalpana and Lee, 2013)
<i>K. pneumoniae</i>	26.84 to 44.42	-	Cube-shape to heterogenous, agglomerated	-	432	2115.35, 1635.60, 3332.78 & 1096.92, cm ⁻¹	(Saleh and Khoman Alwan, 2020)
<i>B. siamensis</i> strain C1	25 to 50 Average:	Ag (91.8%),	Spherical	27.81 (101),	409	3385, 2925, 1732, 1645,	(Ibrahim et al., 2019)

	34±3	Cl (7.5%), S (0.7%)		32.34 (111), 46.29 (200), 57.47 (220), & 77.69 (311)		1556, 1359, 1079 & 537 cm ⁻¹	
<i>B. cereus</i>	2-16		Spherical		420		(Gurunathan, 2019)
<i>K. pneumoniae</i>	22-66	Ag, Cl, C, Na, O, S, N & P	Spherical to irregular	27.6, 32.1, 46.2, 54.7, 57.4 % 76.7 Size: 16.88 nm	475	599, 963, 1299, 1349, 1693, 2299, 2891, & 3780 cm ⁻¹	Current investigation on
<i>M. luteus</i>	21-45	Ag, Cl, C, Na, O, S, N & P	Spherical to irregular	27.6, 32.1, 46.2, 54.7, 57.4 % 76.7 Size: 18	503	599, 963, 1299, 1349, 1693, 2299, 2891, & 3780 cm ⁻¹	Current investigation on

				nm			
<i>E. aerogenes</i>	24-60	Ag, Cl, C, Na, O, S, N & P	Spherical to irregular	27.6, 32.1, 46.2, 54.7, 57.4 % 76.7 Size: 16.44 nm	428	599, 963, 1299, 1349, 1693, 2299, 2891, & 3780 cm ⁻¹	Current investigati on

Table 4(on next page)

Table 4

TABLE 4 The ZOI, tested bacterial species, against different bacterially synthesized AgNPs.

TABLE 4 The ZOI, tested bacterial species, against different bacterially synthesized AgNPs.

Against bacteria	Silver nanoparticles (ZOI in mm)		
	<i>AgNPs- K. pneumoniae</i>	<i>AgNPs- M. leutus</i>	<i>AgNPs- E. aerogenes</i>
<i>B. subtilis</i>	10	11	10
<i>B. cereus</i>	9	8	11
<i>B. megaterium</i>	11	12	8
<i>E. fecalis</i>	11	9	10

Table 5 (on next page)

Table 5

TABLE 5 Summarized form of comparison of antibacterial activity of AgNPs of earlier reported work and current investigation.

TABLE 5 Summarized form of comparison of antibacterial activity of AgNPs of earlier reported work and current investigation.

Tested organism	Synthesized by bacteria	Concentration of AgNPs (µg/mL)	Zone of inhibition (mm)	Method applied	References
<i>E. coli</i> , <i>Ps. aeruginosa</i> , <i>Staph. aureus</i> & <i>B. cereus</i>		50	Lowest	Agar-diffusion method	(Saleh and Khoman Alwan, 2020)
		100			
		150	Highest		
<i>Salmonella enterica</i> , <i>E. coli</i> & <i>S. pyogenes</i>		50 & 100			(Kalpana and Lee, 2013)
		40 to 50 µg/mL			
<i>E. fergusonii</i>	<i>Bacillus cereus</i>	MIC: 7.5		Tube dilution method	(Gurunathan, 2019)
<i>S. mutans</i>		MIC: 9.5			
<i>E. coli</i>	<i>E. coli</i>		10.0		(Peiris et al., 2018)
<i>Ps. aeruginosa</i>	<i>E. coli</i>		10.0		

<i>E. coli</i>	<i>Staph. aureus</i>		14.7		
<i>Ps. aeruginosa</i>			13.0		
<i>Staph. aureus</i>			12.7		
<i>MRSA</i>			12.7		
<i>E. coli</i>	<i>Acinetobacter baumanii</i>		13.3		
<i>Ps. aeruginosa</i>			14.7		
<i>E. coli</i>	<i>Ps. aeruginosa</i>		13.0		
<i>Ps. aeruginosa</i>			12.0		
<i>Staph. aureus</i>			12.3		
<i>MRSA</i>			12.7		
<i>B. subtilis</i>	<i>K. pneumoniae</i>		10	Agar-well diffusion	Current investigation
<i>B. cereus</i>			9		
<i>B. megaterium</i>			11		
<i>E. fecalis</i>			11		
<i>B. subtilis</i>	<i>M. luteus</i>		11		
<i>B. cereus</i>			8		
<i>B. megaterium</i>			12		

<i>E. fecalis</i>			9		
<i>B. subtilis</i>	<i>E. aerogenes</i>		10		
<i>B. cereus</i>			11		
<i>B. megaterium</i>			8		
<i>E. fecalis</i>			10		

3